

# Flavor structure of the unpolarized and longitudinally-polarized sea-quark distributions in the nucleon

M. Wakamatsu\*

*Department of Physics, Faculty of Science,  
Osaka University,  
Toyonaka, Osaka 560-0043, Japan*

## Abstract

It is now widely recognized that a key to unravel the nonperturbative chiral-dynamics of QCD hidden in the deep-inelastic-scattering observables is the flavor structure of sea-quark distributions in the nucleon. We analyze the flavor structure of the nucleon sea in both of the unpolarized and longitudinally polarized parton distribution functions (PDFs) within a single theoretical framework of the flavor SU(3) chiral quark soliton model (CQSM), which contains only one adjustable parameter  $\Delta m_s$ , the effective mass difference between the strange and nonstrange quarks. A particular attention is paid to a nontrivial correlation between the flavor asymmetry of the unpolarized and longitudinally polarized sea-quark distributions and also to a possible particle-antiparticle asymmetry of the strange quark distributions in the nucleon. We also investigate the charge-symmetry-violation (CSV) effects in the parton distribution functions exactly within the same theoretical framework, which is expected to provide us with valuable information on the relative importance of the asymmetry of the strange and antistrange distributions and the CSV effects in the valence-quark distributions inside the nucleon in the resolution scenario of the so-called NuTeV anomaly in the extraction of the Weinberg angle.

---

\* wakamatu@phys.sci.osaka-u.ac.jp

## I. INTRODUCTION

The nucleon structure function physics works out in a fine balance of the perturbative and nonperturbative quantum chromodynamics (QCD). The standard approach to the deep-inelastic-scattering (DIS) physics is based on the so-called factorization theorem, which states that the DIS scattering cross section is factorized into two parts, i.e. the hard part which is tractable within the framework of perturbative QCD and the soft part containing the information of nonperturbative nucleon structure [1] -[4] . Customarily, the soft part is treated as a black box, which should be determined through experiments. This is certainly a reasonable strategy. We however believe that, even if this part is completely fixed by experiments, one would still want to know why those PDFs take the forms so determined. Furthermore, we now realize that a key ingredient to reveal the nonperturbative chiral dynamics of QCD is hidden in the soft part of the DIS physics in the form of the flavor structure (or flavor dependence) of the sea-quark (or anti-quark) distributions [6] -[17]. Unfortunately, what can be extracted from the well-founded inclusive DIS analyses are only the combinations of quark plus sea-quark (or anti-quark) distributions. To separate out anti-quark distributions, we need either of neutrino-induced DIS scattering measurements, semi-inclusive DIS (SIDIS) measurements or Drell-Yan measurements. Because of the smallness of the neutrino-induced DIS cross section, here we are forced to use nuclear targets, which inevitably introduces large theoretical uncertainties in addition to statistical errors arising from the smallness of the event counting rate of neutrino-induced reactions [18] -[24]. On the other hand, a lot of efforts have been made for understanding the SIDIS mechanism [25] -[29], in particular, the fragmentation mechanism of a quark or an antiquark into observed hadrons [30] -[35]. Still, one must say that our understanding of the the semi-inclusive reaction mechanism remains at fairly lower level than that of inclusive reactions. A complementary approach to DIS physics is necessary here to clarify possibly important role of chiral dynamics of QCD in the DIS physics, based on effective models of QCD or on lattice QCD.

Although there are lots of models of baryons, the chiral quark soliton model (CQSM), first proposed by Diakonov, Petrov and Pobylitsa, would probably be the best one [36], at least as an effective model of internal partonic structure of the baryons including the nucleon. (The practical numerical method for handling the CQSM was established in [37] based on the general methodology of Kahana and Ripka [38]. The unique feature of the CQSM, which

plays an important role in the so-called nucleon spin problem, was also pointed out in this paper. For early reviews of the CQSM, see [39] -[42].) The CQSM has a lot of merits over other effective models of baryons. First, it is a relativistic mean-field theory of quarks, with inclusion of infinitely many Dirac-sea orbitals, which means that it is a field theoretical model including infinitely many dynamical degrees of freedom. Second, the mean-field is of hedgehog-shape in harmony with the nonperturbative dynamics expected from large  $N_c$  QCD. One interesting consequence of this unique feature of the model is strong spin-isospin correlation (or anti-correlation) in the generated nucleon seas [37]. Third, in association with the first advantage, its field theoretical nature enables us reasonable estimation not only of quark distributions but also of antiquark distributions [43] - [53]. Last but not least, only one parameter of the flavor SU(2) version of the model, i.e. the dynamically generated quark mass  $M$ , is already fixed to be  $M \simeq 375 \text{ MeV}$  from low energy phenomenology as well as from theoretical ground [36]. To handle the strange-quark degrees of freedom in the nucleon, we must extend the model to flavor SU(3). However, this flavor SU(3) extension of the model need to introduce only one additional parameter, i.e. the mass difference between the strange and nonstrange quarks [52],[53]. This means that we can still make nearly parameter-free predictions for parton distribution functions (PDFs). This should be contrasted with variant species of meson cloud (convolution) models, which are also believed to incorporate the nonperturbative chiral dynamics of QCD. In fact, the meson cloud models contain quite a few model parameters such as several meson-quark coupling constants, coupling form factors, parameters of parton distributions in the mesons, and so forth [54],[55]. Moreover, the model predictions often depend critically on how many meson-baryon intermediate states are included in the theoretical calculations. This last fact is sometimes a serious obstruction for giving unique and quantitatively trustable predictions on the sea-quark distributions in the nucleon. We emphasize again that the CQSM does not suffer from these bothersome problems, because it is nearly parameter-free. As a matter of course, the biggest problem or shortcoming common in all the low energy effective models of the nucleon including the CQSM is a lack of explicit gluon degrees of freedom. This point should always be kept in mind when applying low energy models of the nucleon to the DIS physics, as we shall discuss later.

The main purpose of the present paper is to unravel the nonperturbative chiral dynamics of QCD hidden in the parton distribution functions of the nucleon through the analysis of

the flavor structure of the nucleon seas. An important point is that the flavor structure of the nucleon seas including the strange quark degrees of freedom is analyzed simultaneously for the unpolarized PDFs and for the longitudinally polarized PDFs within a single theoretical framework. It is the flavor SU(3) version of the CQSM, which contains only one adjustable parameter, i.e. the effective mass difference between the strange and nonstrange quarks. To get a feeling about the reliability of the model, we first carry out a systematic comparison between the model predictions and the results of the most recent unbiased global fits by the NNPDF group. In our opinion, this systematic comparison is of special importance. This is because, if one picks up only a specific distribution functions, it would not be extremely difficult to reproduce the corresponding empirical distributions, especially by the models like the meson cloud models containing many parameters as well as freedoms. Unfortunately, it sometimes happens that such an agreement is fortuitous and the same model with the same set of parameters fails to reproduce other independent distributions. This is the reason why we believe it important to check how well a particular model can or cannot reproduce wide class of empirical PDFs simultaneously.

We also investigate the charge-symmetry-violating (CSV) effects in the parton distribution functions based on exactly the same theoretical framework. The motivation to investigate the CSV effects in the nucleon parton distributions is as follows. It is known that, to resolve the widely-known anomaly on the Weinberg angle of the electroweak standard model raised in the analysis of the neutrino-induced DIS measurements by the NuTeV group [56],[57], the two mechanisms of QCD origin are believed to play important roles. They are the asymmetry of the strange and anti-strange quark distributions in the nucleon and the CSV effects in the valence-quark distributions in the proton and the neutron. Which of these ingredients is more important is not a completely settled issue [58] -[72]. We believe that the analysis of the  $s$ - $\bar{s}$  asymmetry and the CSV distributions within a single theoretical framework would provide us with a valuable information on the relative importance of these two mechanisms.

The paper is organized as follows. First, in sect.II, through the comparison of the predictions of the SU(3) CQSM for the unpolarized PDFs with the recent global fits by the NNPDF group [73], we try to estimate the degrees of reliability of the model. After that, we concentrate on inspecting the characteristic feature of the model predictions for flavor structure of the unpolarized light-flavor sea quark distributions, which has not been deter-

mined very reliably on the observational basis alone. The characteristic predictions of the SU(3) CQSM will be compared with the predictions of other models of the sea-quark distributions in the nucleon as well as with other empirical information if available. In sect.III, a similar analysis is carried out for the longitudinally polarized PDFs, the global analyses of which was recently reported by NNPDF group [74]. Next, in sect.IV, we investigate the CSV effects in the light-flavor quark and anti-quark distributions within exactly the same framework of the SU(3) CQSM. A main emphasis there is put on getting useful information on the relative importance of the CSV effects and the strange and anti-strange quark asymmetry in the resolution of the NuTeV anomaly for the Weinberg angle. Then, we summarize what we have learned on the flavor structure of the nucleon seas in sect.V.

## II. FLAVOR SU(3) CQSM AND UNPOLARIZED PDFS

The theoretical formulation of the flavor SU(3) CQSM for evaluating the PDFs in a baryon was already described in detail in our previous papers [52],[53]. (The SU(3) CQSM itself was first proposed in [75].) We therefore give here only a brief sketch of it by confining to its basic theoretical structure. The model lagrangian of the flavor SU(3) CQSM is a straightforward extension of the SU(2) one. It is given by

$$\mathcal{L} = \mathcal{L}_0 + \mathcal{L}_{SB}, \quad (1)$$

where

$$\mathcal{L}_0 = \bar{\psi}(x) (i \not{\partial} - M U^{\gamma_5}(x)) \psi(x), \quad (2)$$

with

$$U^{\gamma_5}(x) = e^{i \gamma_5 \pi(x)/f_\pi}, \quad \pi(x) = \pi_a(x) \lambda_a \quad (a = 1, \dots, 8), \quad (3)$$

being the SU(3) symmetric part of the lagrangian, while

$$\mathcal{L}_{SB} = - \bar{\psi}(x) \Delta m_s P_s \psi(x), \quad (4)$$

with

$$\Delta m_s P_s = \begin{pmatrix} 0 & 0 & 0 \\ 0 & 0 & 0 \\ 0 & 0 & \Delta m_s \end{pmatrix}, \quad (5)$$

being the SU(3) breaking part resulting from the mass difference between the strange and non-strange quarks. (Here, we neglect the light-quark masses so that  $\Delta m_s \equiv m_s - m_{u,d} = m_s$ .) The above effective lagrangian contains eight meson fields instead of three in the case of the flavor SU(2) model. However, we recall that, in the framework of the CQSM, these meson fields are not independent fields of quarks, as inferred from the fact that there is no kinetic term of the meson fields in the above basic lagrangian of the model.

Now, fundamental dynamical assumptions of the model is as follows.

- First, the lowest energy classical solution (or the mean-field solution) is obtained by the embedding of SU(2) mean-field solution of hedgehog shape into the SU(3) matrix. (The same dynamical assumption is also used in more familiar SU(3) Skyrme model [76]-[78].)
- Second is the SU(3) symmetric quantization of the rotational motion in the collective coordinate space.
- The third is the perturbative treatment of the SU(3) symmetry breaking mass term. We recall that this mass difference  $\Delta m_s$  between the strange and nonstrange quarks is *only one parameter* of the model.

We fix this only one parameter of the model is as follows. It is taken as an adjustable parameter between the physically reasonable range  $m_s = (80 - 120)$  MeV. As a general rule, the distribution functions for the light-flavor  $u$ - and  $d$ -quarks are generally rather insensitive to the value of  $\Delta m_s$ . As naturally expected, what are most sensitive to the value of  $\Delta m_s$  is the strange-quark distributions. We found that overall good reproduction of the shape of the empirical strange quark distribution  $s(x) + \bar{s}(x)$  is obtained with the choice  $\Delta m_s = 80$  MeV. We therefore fix the value of  $\Delta m_s$  to be 80 MeV and continue to use it throughout all the following calculations. This means that there remains no more free parameter in the model.

Before going to the discussion on the predictions of the SU(3) CQSM for the unpolarized parton distribution functions (PDFs) in comparison with the empirical information given at the high energy scales, we think it important to explain our general strategy for applying an effective model to DIS physics. It is widely believed that the predictions of effective models of hadrons should be taken as those given in the low energy domain of nonperturbative QCD, while the parton distribution functions extracted from experiments correspond to high

energy scale of perturbative QCD. A difficult question is how to harmonize two domains of QCD. It is customarily assumed that the model predictions for PDFs given at the low energy scale can be related through QCD evolution equation to empirically extracted PDFs at high energy. The central difficulty we encounter here is a matching scale problem. That is, it is far from trivial how to specify the exact model energy scale from which one starts the evolution as above. Most effective models of baryons like the MIT bag model or the meson cloud models use fairly low starting energy  $Q_{ini}^2 \simeq 0.16 \text{ GeV}^2$ . On the other hand, there is some argument that the starting energy of the CQSM should be taken to be a little higher. In fact, we recall here the argument by Petrov et al. based on the instanton picture of the QCD vacuum [79],[80], which is thought to give a theoretical foundation of the CQSM. According to them, the scale of the CQSM is set by the inverse of the average instanton size  $\rho$  as  $Q_{ini} \sim 1/\rho \sim 600 \text{ MeV}$ . Although reasonable, it seems to us that the relation between the choice of initial scale and the average instanton size is very qualitative. It just indicates that any choice between  $Q_{ini}^2 \simeq 0.3 \text{ GeV}^2$  and  $Q_{ini}^2 \simeq 0.4 \text{ GeV}^2$  would be equally well. A fully satisfactory choice of the initial energy scale of evolution would be obtained only when one carries out a proper renormalization procedure of nonperturbative QCD, as is actually done in the framework of lattice QCD, although the calculation of the PDFs is not yet possible in this promising framework. (Another advantage of the lattice QCD treatment is that the renormalization is carried out at fairly high-energy scale, i.e.  $Q^2 = 4 \text{ GeV}^2$ , where one can safely start the perturbative evolution to higher energy scales.) Even though there is a theoretical indication that the model scale of the CQSM is higher than those of other effective models of baryons, it is still much smaller than the scale of  $1 \text{ GeV}$ , so that some sensitivity of the final predictions on the choice of the initial scale of evolution cannot be completely avoided. For instance, we find that the two choices  $Q_{ini}^2 = 0.30 \text{ GeV}^2$  and  $Q_{ini}^2 = 0.40 \text{ GeV}^2$  cause difference in the range of  $(4 \sim 8) \%$  for the heights of valence-like peaks of the unpolarized PDFs at  $Q^2 = 2 \text{ GeV}^2$ . Since better agreement with the empirical PDFs is obtained with the choice  $Q_{ini}^2 = 0.30 \text{ GeV}^2$ , we continue to use this value, which was the value used in our previous studies [50] -[53].

In any case, we emphasize again that the value  $Q_{ini}^2 = 0.30 \text{ GeV}^2$  which we use as the initial scale of evolution in the CQSM is a little higher than the value  $Q_{ini}^2 \simeq 0.16 \text{ GeV}^2$  frequently used in many effective models of baryons like the MIT bag model or the meson cloud models. This difference is sometimes critical, because the validity of using perturbative

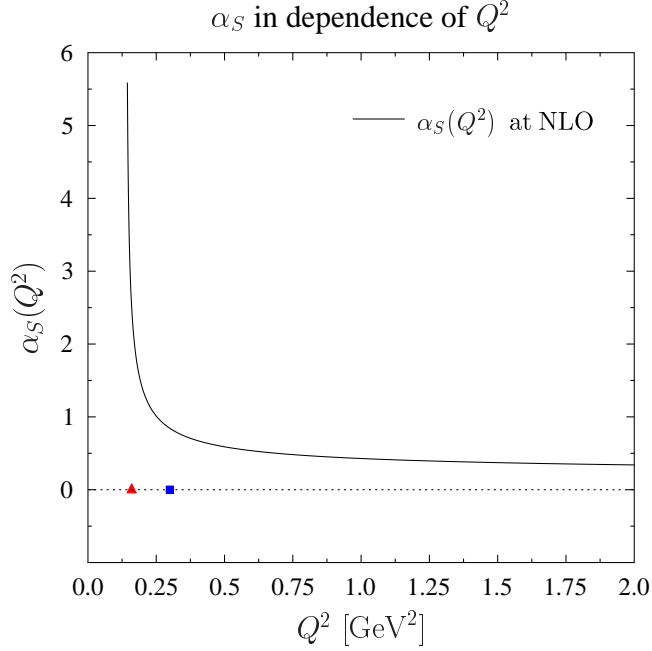


FIG. 1. The QCD running coupling constant  $\alpha_S \equiv g^2 / 4\pi$  at the NLO in dependence of  $Q^2$ . The filled triangle (red in color) corresponds to the frequently used starting energy scale of evolution in the MIT bag model or meson cloud models, whereas the filled square (blue in color) to the starting energy scale used in the CQSM.

evolution equation at too low energy scales is a delicate question. In fact, we show in Fig.1 the QCD running coupling constant at the next-to-leading order (NLO) as a function of  $Q^2$ . (Here we have used the exact solution of the NLO evolution equation with the standard  $\overline{\text{MS}}$  scheme in the fixed-flavor scheme with  $n_f = 3$  even beyond the charm threshold. However, the effects of charm on the quantity discussed here would be very small as compared with the necessary precision of our discussion.) One sees that the  $\alpha_S$  at the scale of  $Q^2 = 0.16 \text{ GeV}^2 = (400 \text{ MeV})^2$  already shows a diverging behavior, which throws a little doubt on the use of the perturbative renormalization group equation at such scales. On the other hand, at the initial energy scale of the CQSM, i.e. at  $Q^2 = 0.30 \text{ GeV}^2 \simeq (550 \text{ MeV})^2$ , the perturbative QCD may be barely applicable. (Whether the value of  $\alpha_S \simeq 0.84$  at the scale  $Q^2 = 0.30 \text{ GeV}^2$  is large or small is a delicate question. However, more transparent measure of the applicability of the perturbative renormalization group equation is provided by the change rate of  $\alpha_S$  as a function of  $Q^2$ , which can be easily read in. Another remark is that, if one uses the LO evolution equation, the diverging behavior of  $\alpha_S(Q^2)$  appears at lower energy scale. This is

one of the reason why many low energy models like the MIT bag model or the meson cloud models adopt the LO evolution equation together with very low starting energy of evolution. However, since the main purpose of our analysis is to compare the predictions of the SU(3) CQSM with the NNPDF fits carried out at the NLO, the consistency requires to use the evolution scheme at the NLO.)

As shown above, although our choice of a little higher starting energy of evolution is preferable from the standpoint of using the scheme of perturbative renormalization group equation, there is one thing which we must pay attention to. The key quantities in our argument here are the momentum fractions of quarks and gluons as functions of the energy scale  $Q^2$ . Up to this time, the momentum fractions of quarks and gluons in the nucleon at the high-energy scale are fairly precisely known. Given below are the empirical values for the quark and gluon momentum fractions  $\langle x \rangle^Q$  and  $\langle x \rangle^G$  given at  $Q^2 = 4 \text{ GeV}^2$  by the MRST2004 analysis [82],[83] :

$$\langle x \rangle^Q = 0.579, \quad \langle x \rangle^G = 0.421. \quad (6)$$

Here, for simplicity, we have neglected very small error bars. As an interesting trial, we carried out a *downward evolution* of the quark and gluon momentum fraction, by starting with these known empirical values at the high energy scale. The results are respectively shown by the solid and the long-dashed curves in Fig.2.

As anticipated, as  $Q^2$  decreases, the quark momentum fraction  $\langle x \rangle^Q$  increases, whereas the gluon momentum fraction  $\langle x \rangle^G$  decreases to eventually become zero at a certain energy scale. An important observation here is the fact that, at the model energy scale of the CQSM, i.e.  $Q^2 = 0.30 \text{ GeV}^2 \simeq (550 \text{ MeV})^2$ , the gluon still carries about 20 % of the nucleon momentum. Since the CQSM is an effective quark model, which does not contain explicit gluon degrees of freedom, to start the evolution at  $Q^2 = 0.30 \text{ GeV}^2$  amounts to neglecting important role of gluons, which are likely to carry about 20 % of the nucleon momentum even at this relatively low energy scale. We will show later that this observation has an important phenomenological consequence in the interpretation of the predictions of the CQSM evolved to the high energy scales.

Before proceeding further, it would be fair to refer to another limitation of the CQSM. The limitation is due to general restriction from the limit of large numbers of colors  $N_c$ . As argued by Diakonov et al. [43],[80], the CQSM provides a practical realization of large- $N_c$

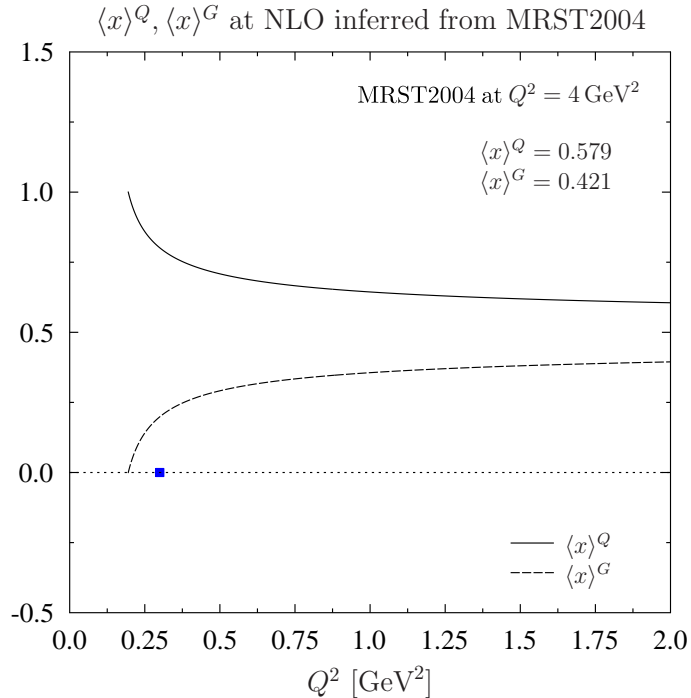


FIG. 2. The quark and gluon longitudinal momentum fractions as functions of  $Q^2$ , obtained by solving the QCD evolution equation at the NLO with the initial conditions  $\langle x \rangle^Q = 0.579$  and  $\langle x \rangle^G = 0.421$  given at  $Q^2 = 4 \text{ GeV}^2$  by the MRST2004 analysis [82],[83]. The filled square (blue in color) corresponds to the starting energy scale used in the CQSM.

QCD, so that the parton distribution functions depend on the Bjorken variable  $x$  in such a way that  $N_c x = O(1)$  in the limit  $N_c \rightarrow \infty$ . Since  $N_c = 3$  in nature, this dictates that the CQSM is a good approximation to QCD only in the region of “not too small”  $x$  in order to comply with the above scaling law. More concrete argument on the applicability range of  $x$  was given in the paper by Petrov et al. [81]. Since the CQSM is an effective theory of QCD, which is not renormalizable, it needs a physical cutoff. An effective regularization energy  $\Lambda_{cut}$  is provided by the inverse of the average instanton size  $\rho$  as  $\Lambda_{cut} \sim 1 / \rho \sim 600 \text{ MeV}$ . Petrov et al. argued that, in the region  $x \leq (M / \Lambda_{cut}) / N_c \simeq 0.1$ , the model predictions for the parton distributions are sensitive to the cutoff energy and/or the detail of the regularization method, so that they are not necessarily reliable. In the following study, we take less ambitious pragmatic standpoint that the CQSM is one of the effective models of baryons like the MIT bag model or the meson cloud models, and will show the predicted PDFs in the whole range of  $x$ , i.e.  $0 < x < 1$ , although the above caution should be kept in mind.

Now we are in a position to compare the predictions of the SU(3) CQSM for the unpolarized PDFs with the empirically extracted ones. First, to get a feeling about the degrees of success or failure of the model, we compare our predictions with the recent unbiased global fits of unpolarized PDFs by the NNPDF group. (Here, we use the NNPDF NLO2.1 fits at the NLO with  $n_f = 3$  [73].) The NNPDF fits are given at  $Q^2 = 2 \text{ GeV}^2$  for the following combinations of the PDFs :

- the singlet distribution,  $\Sigma(x) \equiv \sum_{i=1}^{n_f} (q_i(x) + \bar{q}_i(x))$ ,
- the gluon,  $g(x)$ ,
- the total valence,  $V(x) \equiv \sum_{i=1}^{n_f} (q_i(x) - \bar{q}_i(x))$ ,
- the nonsinglet triplet,  $T_3(x) \equiv (u(x) + \bar{u}(x)) - (d(x) + \bar{d}(x))$ ,
- the sea asymmetry distribution,  $\Delta_S(x) \equiv \bar{d}(x) - \bar{u}(x)$ ,
- the strange anti-strange sum,  $S^+(x) \equiv s(x) + \bar{s}(x)$ ,
- the strange anti-strange difference,  $S^-(x) \equiv s(x) - \bar{s}(x)$ .

For making a comparison, the CQSM predictions given at the initial scale  $Q_{ini}^2 = 0.30 \text{ GeV}^2$  are evolved to the corresponding scale of  $Q^2 = 2 \text{ GeV}^2$  by using the evolution equations at the next-to-leading order (NLO).

Fig.3 show the comparison for the PDFs,  $x T_3(x)$ ,  $x \Delta_S(x)$ ,  $x S^+(x)$ , and  $x S^-(x)$ . We find fairly good agreement between the theory and the NNPDF fits for the flavor nonsinglet triplet distribution  $T_3(x)$  and the light-flavor sea asymmetry  $\Delta_S(x)$ . The detailed inspection reveals that the agreements are not perfect. However, in view of almost parameter-free nature of the model, this agreement can be taken as one of the nontrivial successes of the CQSM, which properly takes account of the chiral dynamics of QCD. (Incidentally, we stress that these distributions  $T_3(x)$  and  $\Delta_S(x)$  are quite insensitive to the value of  $\Delta m_s$ .)

Turning to the strange distributions, we find that the model prediction for  $S^+(x) = s(x) + \bar{s}(x)$  appears to overestimate the NNPDF fit roughly by a factor of two. This feature of the model prediction could be anticipated. As was intensively discussed for the SU(3) Skyrme model, the SU(3) symmetric collective quantization supplemented with the

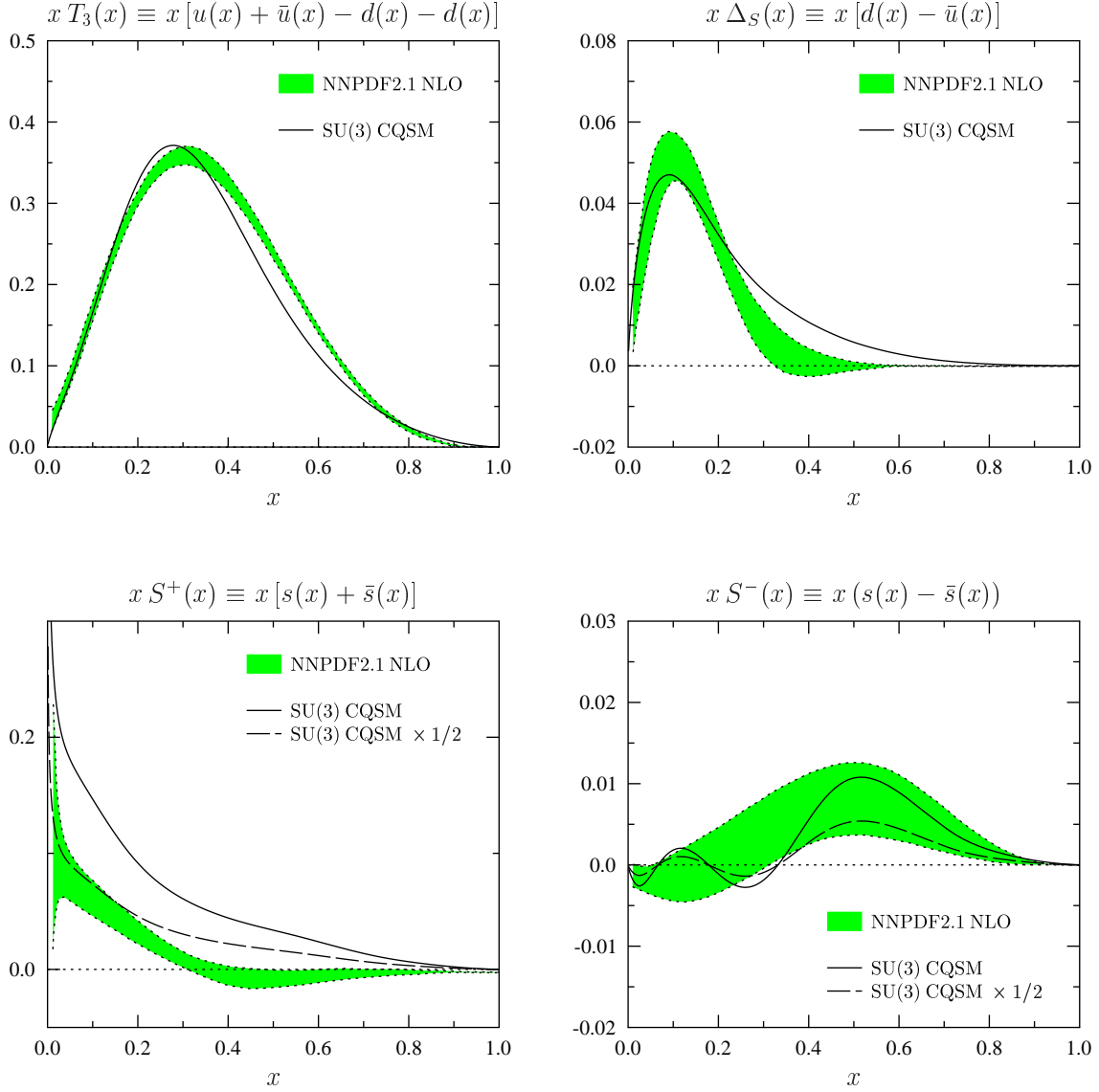


FIG. 3. The predictions of the SU(3) CQSM for the nonsinglet and strange quark distributions evolved from  $Q_{ini}^2 = 0.30 \text{ GeV}^2$  to  $Q^2 = 2 \text{ GeV}^2$  in comparison with the NNPDF2.1 NLO global fits shown by the shaded areas [74]. The solid curves are the predictions of the SU(3) CQSM. The long-dashed curves for the strange quark distribution are the reduced predictions of the SU(3) CQSM by a factor of 1/2 explained in the text.

perturbative treatment of the SU(3) breaking mass difference term, which is taken over to our treatment of the SU(3) CQSM, has a danger of overestimating the effects of kaon clouds, which might in turn lead to an overestimation of the strange quark components in the nucleon [86]-[88]. We conjecture that plausible predictions for the strange and anti-strange

distributions in the nucleon would lie just between the predictions of the SU(3) CQSM and the SU(2) CQSM, which amounts to multiplying a reduction factor 1/2 to the SU(3) CQSM predictions for  $s(x)$  and  $\bar{s}(x)$ . As a matter of fact, the reduction factor of just 1/2 has no strict foundation and rather ad hoc. It can be any number between 1 and 0. In principle, this reduction factor can be treated as additional parameter of the model. However, there is no absolutely trustworthy empirical information to fix this parameter. We therefore simply say that, as seen from Fig.3, after multiplying this reduction factor of 1/2, the model prediction for  $S^+(x)$  is order of magnitude consistent with the current NNPDF fit, except for larger  $x$  region, where the NNPDF fit does not necessarily respect the positivity of the distribution.

Also very interesting is the asymmetry of strange and anti-strange distributions. Noteworthy feature of the NNPDF fit is that the difference distribution  $xS^-(x) \equiv x[s(x) - \bar{s}(x)]$  has a peak around  $x \sim 0.5$ . Very curiously, this feature is perfectly consistent with the prediction of the SU(3) CQSM. The good agreement is not limited to the position of the peak. The absolute magnitude of the asymmetry is also consistent with the NNPDF fit. Note that the bare prediction of the SU(3) CQSM and the reduced prediction by a factor of 1/2 are both consistent with the NNPDF fit within the uncertainty band, although we prefer the reduced prediction.

Next, in Fig.4, we show the model predictions for the singlet distribution  $\Sigma(x)$ , the gluon distribution  $g(x)$ , and the net valence distribution  $V(x)$ , in comparison with the NNPDF fits. As compared with the success for the nonsinglet distributions, we find that the model prediction overestimates the NNPDF fit by about 20 %. The reason of this discrepancy may be interpreted as follows. We already pointed out that, at the starting energy scale of evolution, the gluon field is likely to carry about 20 % of the total nucleon momentum, which means that the quark fields carry only about 80 % of the nucleon momentum. On the other hand, the CQSM is an effective quark model, which does not contain explicit gluon degrees of freedom, the net nucleon momentum is naturally saturated by the momenta of quarks and anti-quarks at the model scale. Thus, we simply had to set the gluon distribution to be zero at the starting energy scale of evolution, i.e. at  $Q_{ini}^2 = 0.30 \text{ GeV}^2$ . This naturally fails to take account of the fact that the net momentum fraction of quarks at the initial scale must be only about 80 %, which would then lead to an overestimation of the flavor singlet combination of the quark and anti-quark distribution  $\Sigma(x)$  by about 20 %. By the same reason, we cannot expect that the model can give a reasonable description of the

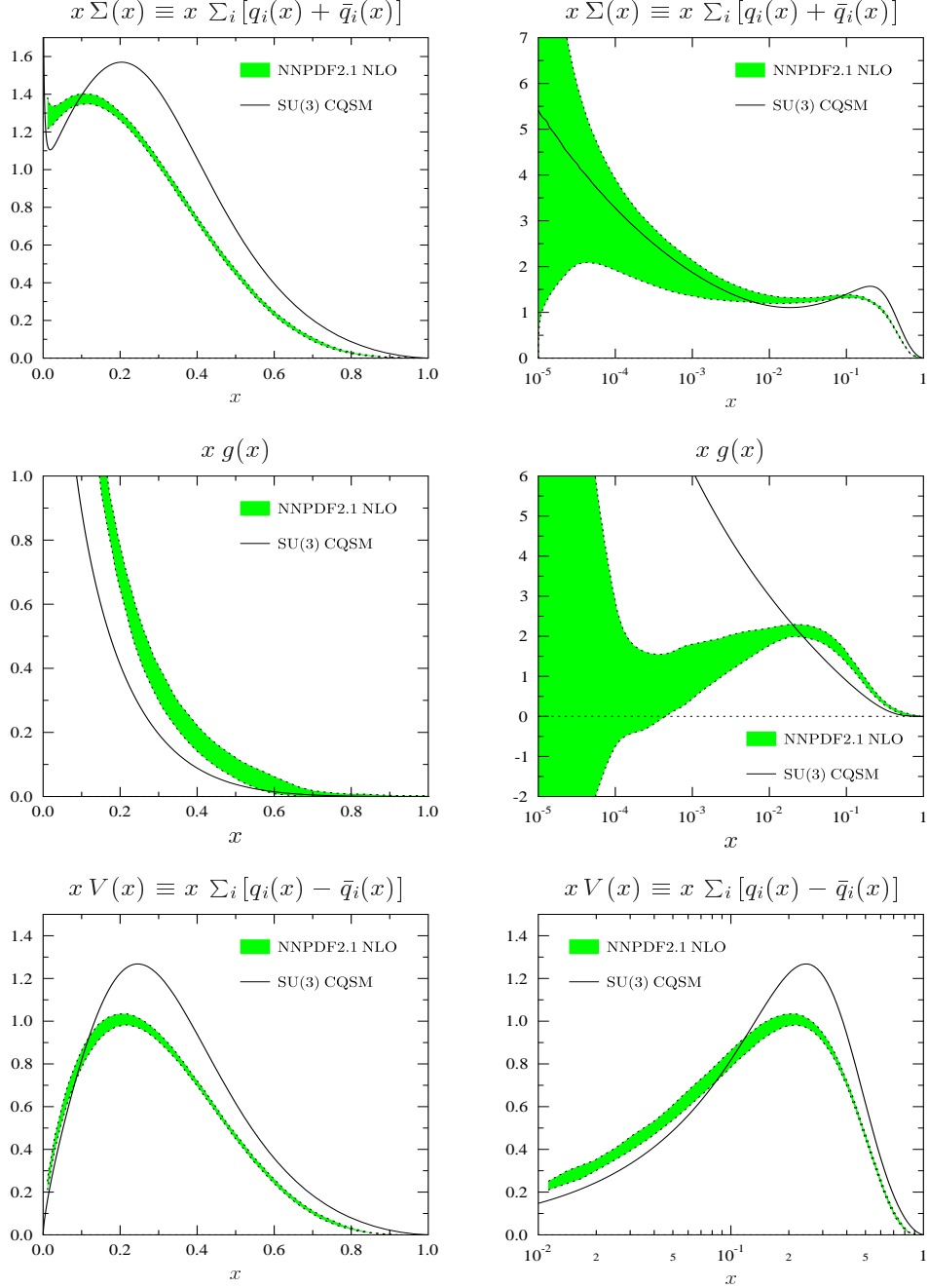


FIG. 4. The SU(3) CQSM predictions for the singlet quark, gluon and valence quark distributions in comparison with the NNPDF2.1 NLO fits.

gluon distribution even though nonzero gluon distribution is generated through evolution. Naturally, the gluon distribution obtained in this way has no valence-like peak as observed in the empirical fit.

Turning to the total valence distribution  $V(x)$ , one again observes that the model pre-

diction overestimates the NNPDF fit by about 20 %. The reason of this overestimation is slightly more complicated than the singlet distribution  $\Sigma(x)$ . Since this distribution  $V(x)$  is given as a difference of the quark and anti-quark distributions, it does not couple to the gluon distribution at the process of scale evolution different from the distribution  $\Sigma(x)$ . Still, since it is a symmetric sum of the three flavors,  $u$ ,  $d$ , and  $s$ , the possible overestimation of the net distribution at the initial energy scale pointed out before is likely to remain also at higher energy scales. Another possible reason would be that the model might still underestimate the sum of the light-flavor sea quark distributions, i.e.,  $\bar{u}(x) + \bar{d}(x)$ , which leads to the overestimation of the combination  $u(x) - \bar{u}(x) + d(x) - \bar{d}(x) + s(x) - \bar{s}(x)$ , provided that the contribution of  $s(x) - \bar{s}(x)$  in this combination is small.

A lesson learned from the above analysis is as follows. The overall agreement between the SU(3) CQSM and the NNPDF2.1 NLO fits are fairly good in view of nearly parameter-free nature of the model predictions. However, the agreement is not naturally perfect. The main reason of discrepancy would be the neglect of the gluon degrees of freedom, which appears to play non-negligible roles in the flavor-singlet channel even at relatively low energy scales. On the other hand, we shall see in the next section that the role of gluons at the low energy model scale of the CQSM is likely to be much less important in the case of longitudinally polarized distributions.

After having got a feeling on the degrees of reliability of the model as well as its limitation, through the comparison with the unbiased global fits of the unpolarized PDFs by the NNPDF groups, we now turn our attention to more detailed inspection on the flavor structure of the sea-quark (anti-quark) distributions in the nucleon. To unravel the underlying physics, particularly instructive here is a comparison with related theoretical investigations as well as other experimental information if available. First, we call attention to the strange distribution  $s(x) + \bar{s}(x)$  in the nucleon extracted from the analysis of charged kaon production in semi-inclusive DIS (SIDIS) by the HERMES group [25]. As is widely known, the extracted  $s(x) + \bar{s}(x)$  distribution appears to have intriguing two-component structure as illustrated in Fig.5. Here, following the paper [89], the HERMES data with  $x < 0.1$  are represented by the open circles, while those with  $x > 0.1$  are by the filled black circles just by the reason of guidance for eye.

The observed two-peaked structure motivates Chang and Peng to introduce an interesting

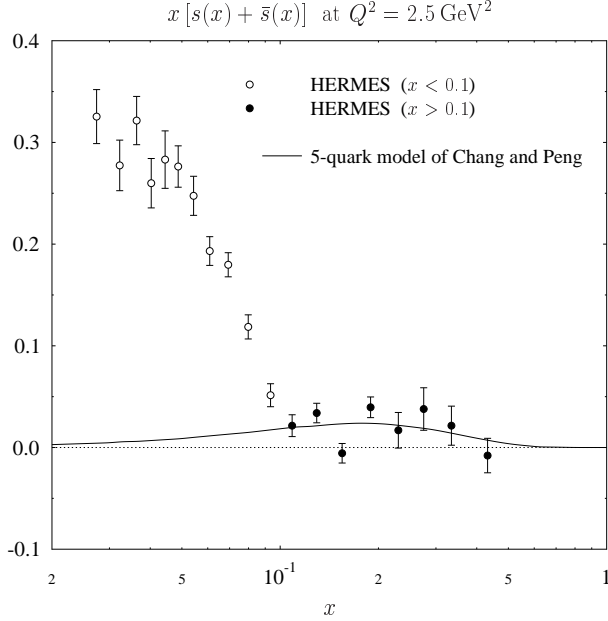


FIG. 5. HERMES strange quark distribution [25] in comparison with the prediction of the 5-quark model of Chang and Peng [89], evolved to  $Q^2 = 2.5 \text{ GeV}^2$  from the initial scale of the model  $Q_{ini}^2 = 0.25 \text{ GeV}^2$ .

physical interpretation to be explained below [89]. (See also more recent paper by Chang, Cheng, Peng and Liu [90].) Their interpretation is based on the idea of intrinsic charm in the nucleon proposed many years ago by Brodsky, Hoyer, Petesen, and Sakai [91],[92] (BHPS model). According to BHPS, the intrinsic sea is a component that is expected to have valence-like peak at larger  $x$ , while the extrinsic sea is thought to be generated through QCD splitting processes. Inspired by this idea, Chang and Peng et al. proposed an idea that  $x > 1$  HERMES data are dominated by “intrinsic” sea, while  $x < 0.1$  data from “extrinsic” sea [89]. According to them, a component of the HERMES data, which has a peak around  $x \sim (0.1-0.3)$  can be reproduced by the intrinsic 5-quark model (see the solid curve in Fig.5) with the mixing rate  $P_5^{uuds\bar{s}} \simeq 0.024$  of the 5-quark component in the nucleon. At first sight, this appears to provide a reasonable explanation of the peak structure of  $x [s(x) + \bar{s}(x)]$  in the higher  $x$  region. However, the following question immediately arises. Admitting that the account of the 5-quark component nicely explains the peak structure at higher  $x$ , how can one explain the sea-like component in the lower  $x$  domain? What is important to recognize here is the fact that the solid curve in Fig.5 shows the theoretical prediction, which was obtained

after taking account of the evolution effects by solving the evolution equation starting from the scale  $Q_{ini}^2 = 0.25$  GeV. This means that, to explain the whole HERMES data including the lower  $x$  behavior, one absolutely need a significant sea-like component already at the starting energy scale. What generate these sea-like components ? Assuming the correctness of the HERMES extraction, they must be higher Fock-components of the nucleon state like the 7-quark component, 5-quark plus gluon, and so on. It is not absolutely clear whether the valence-like peak structure of the strange quark distribution, which is obtained by confining to the lowest 5-quark Fock-component only, will remain or not after taking account of all the these higher Fock-components of the nucleon wave function.

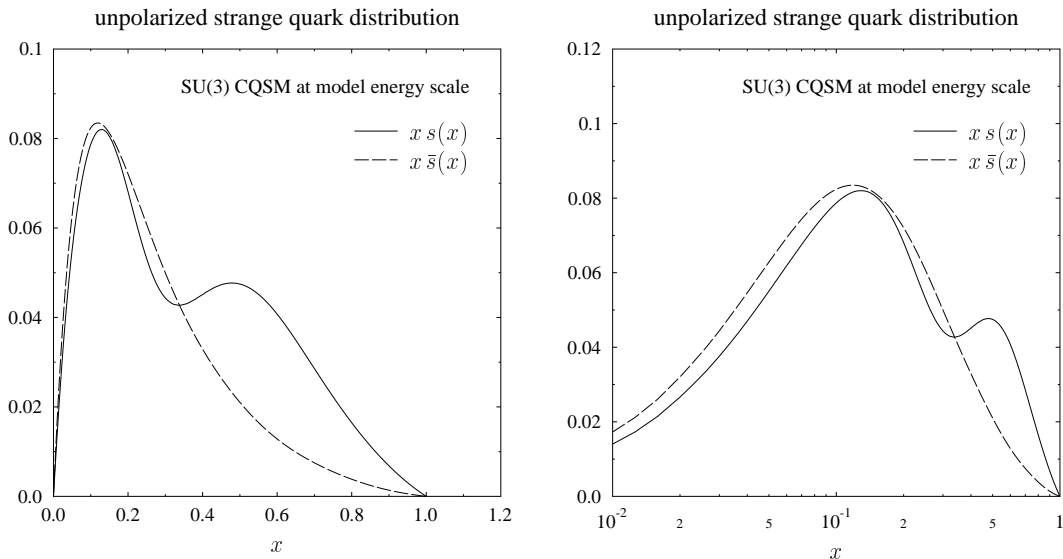


FIG. 6. The SU(3) CQSM predictions for the strange and anti-strange distribution in the nucleon at the model energy scale. The left panel is in linear scale in  $x$ , while the right panel is in log scale.

To answer the question raised above, we find it useful to look into the prediction of the SU(3) CQSM for the strange and anti-strange distribution functions at the low energy model scale. They are shown in Fig.6. Very interestingly, the model predicts a sizable difference between the strange and anti-strange quark distributions. The strange quark distribution  $x s(x)$  shows a two-component structure, i.e. the valence-like peak in the higher  $x$  region and the sea-like component in the lower  $x$  region. On the other hand, the anti-strange quark distribution has only a sea-like peak in the lower  $x$  region. In particular, one finds that the  $s$ -quark distribution has larger  $x$  component than the  $\bar{s}$ -quark distribution. Very interestingly,

this is just a feature expected from the kaon cloud model of the nucleon advocated by Signal and Thomas [58], Burkardt and Warr [59], and also by Brodsky and Ma [60] many years ago. According to the kaon cloud picture, the strange and anti-strange quark distributions in the proton are generated through the virtual dissociation process  $p \rightarrow \Lambda + K^+$ . In this virtual intermediate states, the  $s$ -quark is contained in a baryon, i.e. in  $\Lambda$ , while the  $\bar{s}$ -quark is contained in a meson, i.e. in  $K^+$ . This is expected to explain that the  $s$ -quark has valence-like harder component than  $\bar{s}$ -quarks [59],[60]. Although we believe that this meson cloud picture gets straight to the point in a qualitative sense, its quantitative predictability cannot be expected too much, because the meson cloud models generally contain too many adjustable parameters and large ambiguities. A great advantage of the CQSM is that it does not assume any explicit meson-baryon intermediate states like the nucleon and pion, the nucleon and rho meson, and the lambda and kaon, etc. Note that the above difference between the strange and anti-strange quark distributions is an automatic consequence of almost parameter-free calculation. Here, it is very important to recognize the fact that not only the valence-like component but also the sea-like component are generated as a consequence of solving the bound state equation of the nucleon. In this sense, one can call the latter too as “intrinsic” sea not “extrinsic” sea, even though it is not a component with valence-like character. The point is that the basic theoretical framework of the CQSM is the mean-field theory (followed by the collective quantization of the zero-energy rotational modes), which enables us to incorporate infinitely many higher multi-quark components in the language of perturbative Fock-space expansion. This argument indicates that the decomposition of the quark seas into the “intrinsic” and the “extrinsic” components is a strongly model-dependent or theoretical-scheme-dependent idea.

Also interesting here is the effect of evolution. We show in Fig.7 the prediction of the SU(3) CQSM evolved to  $Q^2 = 2.5 \text{ GeV}^2$  corresponding to the HERMES SIDIS extraction of the distribution  $x [s(x) + \bar{s}(x)]$ . One sees that the trace of the valence-like peaked structure of the distribution  $x s(x)$  still remains faintly. However, it is smoothly connected to the sea-like structure in the lower  $x$  domain. Accordingly, we do not see clear two-component structure in  $x s(x)$  any more. On the other hand, since the distribution  $x \bar{s}(x)$  has only a sea-like component even at the low energy model scale, the evolved distribution is simply sea-like.

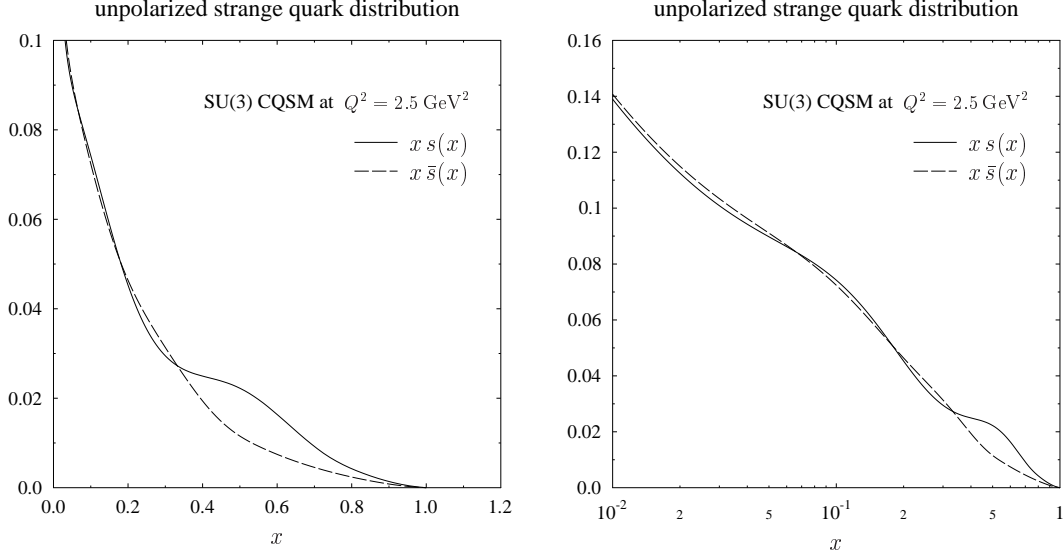


FIG. 7. The SU(3) CQSM predictions for the strange and anti-strange distribution in the nucleon evolved to  $Q^2 = 2.5 \text{ GeV}^2$ . The left panel is in linear scale in  $x$ , while the right panel is in log scale.

After these considerations, it is instructive to compare the prediction of the strange plus anti-strange quark distribution with the corresponding HERMES extraction as well as several other global fits. The filled black circles in Fig.8 stand for the HERMES SIDIS extraction for  $x[s(x) + \bar{s}(x)]$ . The thicker shaded area represents the NNPDF global fit given at  $Q^2 = 2.0 \text{ GeV}^2$ , while the thinner shaded area does the CTEQ6.5 fit corresponding to  $Q^2 = 2.5 \text{ GeV}^2$ . (Here, the NNPDF fit corresponds to slightly lower scale, but the effect of this difference is expected to be small as compared with sizably large difference with the CTEQ6.5 fit.) The newer CT10 fit is also shown for reference by the dash-dotted curve for reference. The bare prediction of the SU(3) CQSM is shown by the solid curve, whereas the reduced prediction of the SU(3) CQSM is by the long-dashed curve. (By the reason already explained, we prefer the reduced prediction for the strange quark distributions.) As pointed out above, the SU(3) CQSM prediction for  $x[s(x) + \bar{s}(x)]$  at  $Q^2 = 2.5 \text{ GeV}^2$  does not show any clear two-component structure, which is indicated by the HERMES data. Note that this is also a common feature of all the global fits including the NNPDF group and the CTEQ group. As is well known, the HERMES extraction of the strange distribution heavily depends on the expectation that our understanding of the semi-inclusive charged-kaon production mechanism is robust enough. Actually, the small- $x$  data in the

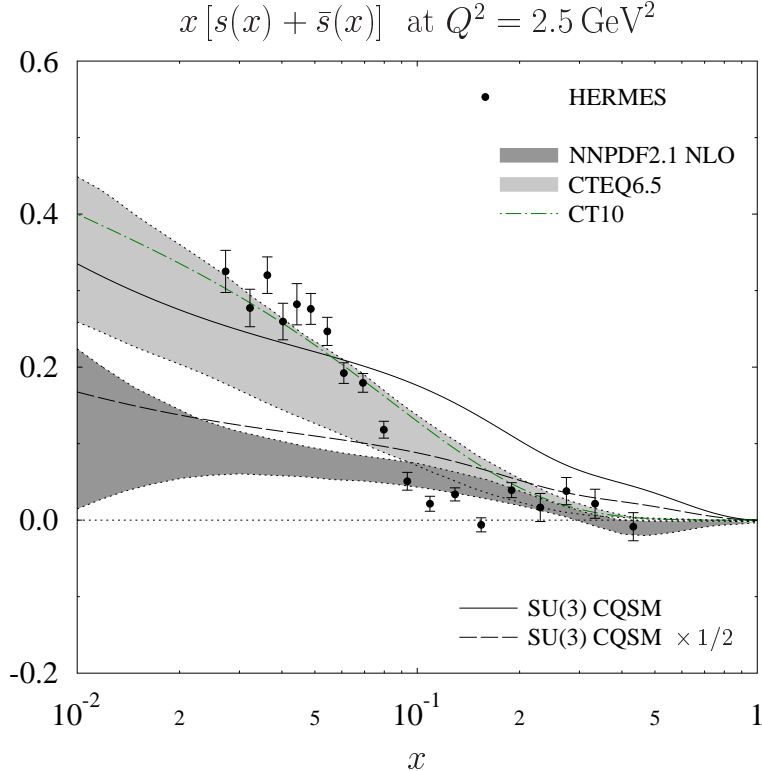


FIG. 8. The SU(3) CQSM predictions for the strange and anti-strange distribution at  $Q^2 = 2.5 \text{ GeV}^2$  in comparison with the HERMES SIDIS extraction [25]. The solid curve stands for the bare prediction of the SU(3) CQSM, whereas the dashed curve is the reduced prediction of the same model by a factor of  $1/2$ . The global fits by the NNPDF group given at  $Q^2 = 2 \text{ GeV}^2$  and the two global fits by the CTEQ group corresponding to  $Q^2 = 2.5 \text{ GeV}^2$  are also shown for comparison [93],[94].

HERMES extraction corresponds to relatively low energy kinematical region, say,  $Q^2 \sim 1 \text{ GeV}^2$ , where one would generally expect fairly large higher twist corrections to the DIS analysis. Still another problem pointed out by Leader, Sidorov, and Stamenov is that the HERMES analysis uses the factorized QCD treatment of the data in kinematical region where it is not necessarily justified [95]. We also point out that the most recent HERMES analysis [96], which is claimed to confirm their earlier analysis [25], was criticized in a recent paper by Stolarski [97]. Stolarski emphasized the importance of carrying out a careful analysis in which not only the multiplicity sum of the kaon but also that of the pions as well as other combinations of  $K^+$  and  $K^-$  multiplicities are analysed simultaneously. In any case,

we strongly feel that some totally independent extraction of the strange quark distributions, for example, by using the neutrino-induced inclusive DIS measurements, is highly desirable.

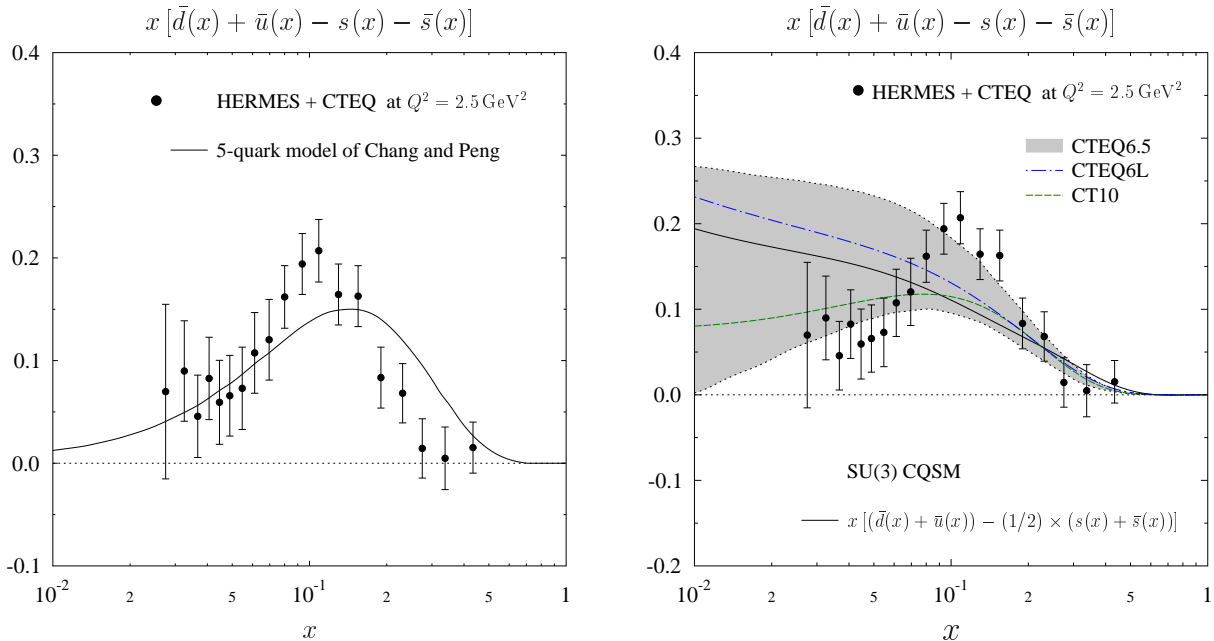


FIG. 9. The distribution  $x [\bar{u}(x) + \bar{d}(x) - s(x) - \bar{s}(x)]$  obtained by using the CTEQ6.6 global fit for  $\bar{u} + \bar{d}$  [93] and the HERMES SIDIS data for  $s + \bar{s}$  [25]. The left panel shows the comparison with the prediction of the BPHS 5-quark model due to Chang and Peng [98], while the right panel does the comparison with the prediction of the SU3 CQSM as well as some other global fits [93],[94].

Chang and Peng pushed their idea of “intrinsic” sea still forward by considering the combination of the distributions  $\bar{u}(x) + \bar{d}(x) - s(x) - \bar{s}(x)$  [98]. According to them, this combination of the distribution is particularly interesting, because the contribution from the “extrinsic” seas is expected to just cancel in this combination, so that it is only sensitive to the “intrinsic” sea. Their analysis then goes as follows. First, they proposed to extract this distribution in an empirical way, i.e. by using the HERMES SIDIS data for  $x [s(x) + \bar{s}(x)]$  at  $Q^2 = 2.5 \text{ GeV}^2$  [25] and the CTEQ6.6 fit for the distribution  $x [\bar{u}(x) + \bar{d}(x)]$  at the same scale [93] as

$$x [\bar{u}(x) + \bar{d}(x) - s(x) - \bar{s}(x)] \Rightarrow x [\bar{u}(x) + \bar{d}(x)]_{\text{CTEQ6.6}} - x [s(x) + \bar{s}(x)]_{\text{HERMES}}. \quad (7)$$

The resultant distribution is plotted by the filled circles in the left panel of Fig.9. A prominent feature of the so-obtained  $x [\bar{u}(x) + \bar{d}(x) - s(x) - \bar{s}(x)]$  appears to have an expected

valence-like peaked structure. Next, they calculated the corresponding distribution on the basis of the BHPS model [91],[92], which gives

$$\bar{u}(x) + \bar{d}(x) - s(x) - \bar{s}(x) = P^{u\bar{u}}(x_{\bar{u}}) + P^{d\bar{d}}(x_{\bar{d}}) - 2P^{s\bar{s}}(x_{\bar{s}}). \quad (8)$$

where  $P^{Q\bar{Q}}(X_{\bar{Q}})$  is the  $x$  distribution of  $\bar{Q}$  in the Fock component  $|uudQ\bar{Q}\rangle$  of the nucleon state vector. In this calculation, they assumed that the probability of the intrinsic sea is proportional to  $1/m_Q^2$  with  $m_Q$  being the mass of quark (antiquark)  $Q$ . This BHPS prediction is then evolved to  $Q^2 = 2.5 \text{ GeV}^2$  by taking  $Q_{ini}^2 = (0.5 \text{ GeV})^2$  as the initial energy scale of evolution. The answer is shown by the solid curve in the left panel of Fig.9. Chang and Peng emphasized that the qualitative agreement between the data and the calculation provides strong supports to the existence of the intrinsic  $u$  and  $d$  quark seas and also to the adequacy of the BHPS idea.

We point out that the valence-like peaked structure of the empirically extracted distribution  $x [\bar{u}(x) + \bar{d}(x) - s(x) - \bar{s}(x)]$  may critically depend on the following two factors,

- the two-component structure of the HERMES SIDIS data for  $x [s(x) + \bar{s}(x)]$  :
- the relative magnitudes of the sea-like components of the  $\bar{u} + \bar{d}$  distribution and the  $s + \bar{s}$  distribution in the lower  $x$  domain.

To confirm it, we first check what happens if we do not use the HERMES SIDIS data for the strange quark distribution. In fact, from the viewpoint of internal consistency, it would be more legitimate to extract the distribution in question by using the same set of extraction framework for both of  $x [\bar{u}(x) + \bar{d}(x)]$  and  $x [s(x) + \bar{s}(x)]$ . The dotted and dash-dotted curves in the right panel of Fig.9 respectively correspond to the results obtained by using the CTEQ6L fit [93] and the CT10 fit [94]. One finds a big difference between these two fits. The distribution obtained from the CT10 fit has a peaked structure, whereas that obtained from the CTEQ6L does not. The origin of this difference can primarily be traced back to the relative magnitudes of the  $s + \bar{s}$  and  $\bar{u} + \bar{d}$  distributions in the lower  $x$  region. (We point out that the CT10 fit gives larger magnitude of  $s + \bar{s}$  distribution than the CTEQ6L fit and also the NNPDF fit.) For reference, we also show in the right panel of Fig.9 the prediction of the CQSM by the long-dashed curve. By the reason explained before, we have used the reduced prediction for the  $x [s(x) + \bar{s}(x)]$  distribution. It is interesting to see that the resultant distribution  $x [\bar{u}(x) + \bar{d}(x) - s(x) - \bar{s}(x)]$  is remarkably similar in shape to

that of the CTEQ6L fit, which does not show a peaked structure. In any case, all these theoretical and semi-empirical predictions for the distribution  $x [\bar{u}(x) + \bar{d}(x) - s(x) - \bar{s}(x)]$  lie within the wide uncertainty band indicated by the CTEQ6.5 fit, which in fact allows both of the peaked and peak-less structures. Undoubtedly, to get more confident information on the  $x$ -dependence of this interesting combination  $x [\bar{u}(x) + \bar{d}(x) - s(x) - \bar{s}(x)]$ , we need to get more reliable separate information for the light-flavor sea-quark distribution  $x [\bar{u}(x) + \bar{d}(x)]$  and the strange quark distribution  $x [s(x) + \bar{s}(x)]$  in the nucleon.

An interesting idea of “two component” quark sea was also advocated by Liu and the collaborators based on the path-integral formulation or within the framework of the lattice QCD [90],[99],[100]. According to them, the light-flavor  $u$ - and  $d$ -quark seas consist of the connected sea and the disconnected sea, while the strange as well as charm sea comes only from disconnected sea. On the basis of this idea, they carried out a phenomenological extraction of the connected and disconnected pieces of the light-flavor sea,  $\bar{u}(x) + \bar{d}(x)$ . They first assume that the disconnected sea component of the  $\bar{u}(x) + \bar{d}(x)$  distribution is proportional to the  $s(x) + \bar{s}(x)$  distribution as

$$\bar{u}^{ds}(x) + \bar{d}^{ds}(x) = \frac{1}{R} [s(x) + \bar{s}(x)], \quad (9)$$

with the proportional constant

$$R = \frac{\langle x \rangle_{s+\bar{s}}}{\langle x \rangle_{u+\bar{u}} (DI)} = \frac{\langle x \rangle_{s+\bar{s}}}{\langle x \rangle_{\bar{u}^{ds}+\bar{d}^{ds}}} = 0.857(40). \quad (10)$$

which they estimated from lattice data. Then, they extracted the connected sea (CS) component of the  $\bar{u}(x) + \bar{d}(x)$  distribution, by using the CT10 PDF fit for  $\bar{u}(x) + \bar{d}(x)$  and the HERMES SIDIS data for the strange quark distribution  $s(x) + \bar{s}(x)$  as

$$\begin{aligned} \bar{u}^{cs}(x) + \bar{d}^{cs}(x) &\equiv [\bar{u}(x) + \bar{d}(x)] - [\bar{u}^{ds}(x) + \bar{d}^{ds}(x)] \\ &= [\bar{u}(x) + \bar{d}(x)]_{\text{CT10}} - \frac{1}{R} [s(x) + \bar{s}(x)]_{\text{HERMES}}. \end{aligned} \quad (11)$$

The connected and disconnected seas for  $\bar{u} + \bar{d}$  extracted from the above-explained phenomenological analysis are shown in Fig.10 by the filled square (red in color) and the filled circles (black in color), respectively. Note that, by construction, the sum of these two components, i.e. the connected sea and the disconnected sea, coincides with the CT10 global fit shown by the dash-dotted curve. They emphasize that the connected sea component so

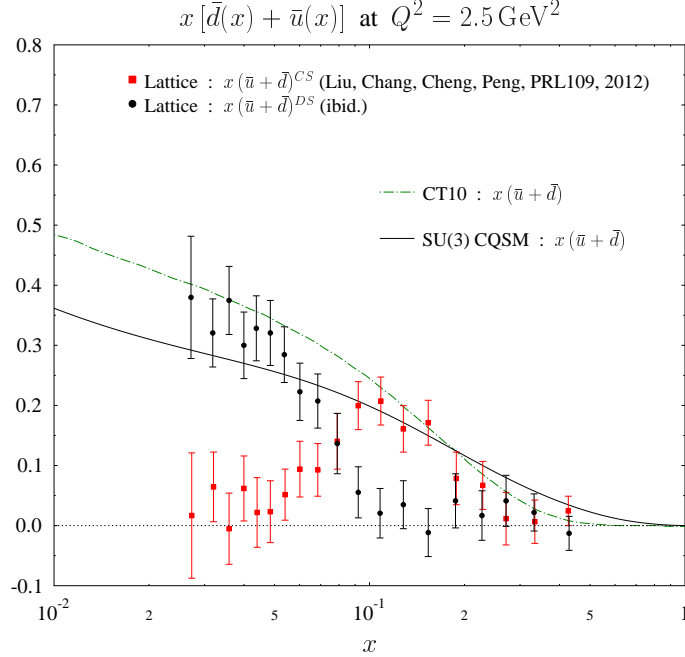


FIG. 10. The connected (filled circles) and disconnected (filled squares) seas for  $\bar{u}(x) + \bar{d}(x)$  extracted from CT10 PDF fit for  $\bar{u}(x) + \bar{d}(x)$  [94] and the HERMES SIDIS data for the strange quark distribution  $s(x) + \bar{s}(x)$  [25], under the assumption that the disconnected sea component of the  $\bar{u}(x) + \bar{d}(x)$  distribution is proportional to the  $s(x) + \bar{s}(x)$  distribution [90].

extracted appears to have a valence-like peak around  $x \simeq (0.1 - 0.2)$ . However, it seems to us that their separation into the two components is not also independent on the structure of the HERMES data for the strange quark distribution. Going back to the original physical idea of Liu et al. [99],[100], it is certainly true that the distribution  $\bar{u}(x) + \bar{d}(x)$  is generally given as a sum of the connected and disconnected sea contributions. This reminds us of the similar idea of Chang and Peng [89],[98]. In their language, it roughly corresponds to saying that the distribution  $\bar{u}(x) + \bar{d}(x)$  consists of “intrinsic” sea and “extrinsic” sea. However, it should be recognized that there is no rigorous correspondence between the two terminologies, i.e. the idea of “intrinsic” and “extrinsic” seas and that of connected and disconnected seas in the language of the lattice QCD. In fact, according to Chang and Peng, the strange quark distribution  $x[s(x) + \bar{s}(x)]$  also contains the “intrinsic” component. But, this “intrinsic” sea requires at least 5-quark component, which needs to take account of disconnected seas within the framework of lattice QCD.

In our opinion, just like that the decomposition into the “intrinsic” sea and the “intrinsic”

is a model-dependent idea, the decomposition into the connected sea and the disconnected sea is an idea, which has a definite meaning only within the framework of the lattice QCD formulation of QCD. Model independent notion is only the separation into a quark and anti-quark distributions. In fact, we show in Fig.10 also the prediction of the SU(3) CQSM for  $x [\bar{u}(x) + \bar{d}(x)]$  by the solid curve. Although it slightly underestimates the magnitude of  $\bar{u} + \bar{d}$  in the small  $x$  region as compared with the CT10 global fit [94], an important fact is that it does not show any two-component structure just like the CT10 fit does not. Furthermore, within the framework of the CQSM, there is no idea of decomposing the anti-quark distributions into the two components like the “intrinsic” and “extrinsic” sea. Both are contained within a single theoretical scheme without any separation between them. This reconfirms again that the separation of the anti-quark distribution into the “intrinsic” and “extrinsic” components or into the connected and disconnected seas is a *theoretical-scheme-dependent idea*, although we never deny its usefulness for understanding the nature quark seas in the nucleon.

### III. FLAVOR SU(3) CQSM AND LONGITUDINALLY POLARIZED PDFS

In this section, we compare the predictions of the SU(3) CQSM for the longitudinally-polarized PDFs with empirically extracted ones. Similarly as for the unpolarized PDFs, to get a feeling about the degrees of success or failure of the model, we first compare our predictions with the recently reported global fits of the longitudinally polarized PDFs by the NNPDF group, i.e. NNPDFpol1.0 [74]. The NNPDF fits for the longitudinally polarized PDFs are given at  $Q^2 = 1 \text{ GeV}^2$  for the following combinations of the PDFs :

- the flavor singlet,  $\Delta\Sigma(x) \equiv \sum_{i=1}^{n_f} (\Delta q_i(x) + \Delta \bar{q}_i(x))$ ,
- the gluon,  $\Delta g(x)$ ,
- the isospin triplet,  $\Delta T_3(x) \equiv (\Delta u(x) + \Delta \bar{u}(x)) - (\Delta d(x) + \Delta \bar{d}(x))$ ,
- the SU(3) octet,  $\Delta T_8(x) \equiv \Delta u(x) + \Delta \bar{u}(x) + \Delta d(x) + \Delta \bar{d}(x) - 2(\Delta s(x) + \Delta \bar{s}(x))$ ,
- the  $u$  plus  $\bar{u}$ ,  $\Delta u(x) + \Delta \bar{u}(x)$ ,
- the  $d$  plus  $\bar{d}$ ,  $\Delta d(x) + \Delta \bar{d}(x)$ ,

- the  $s$  plus  $\bar{s}$ ,  $\Delta s(x) + \Delta \bar{s}(x)$ .

For making a comparison, the CQSM predictions are evolved from the initial scale  $Q_{ini}^2 = 0.30 \text{ GeV}^2$  to the scale  $Q^2 = 1.0 \text{ GeV}^2$  where the NNPDF fits are given. As before, the gluon distribution at the initial scale is simply set to be zero.

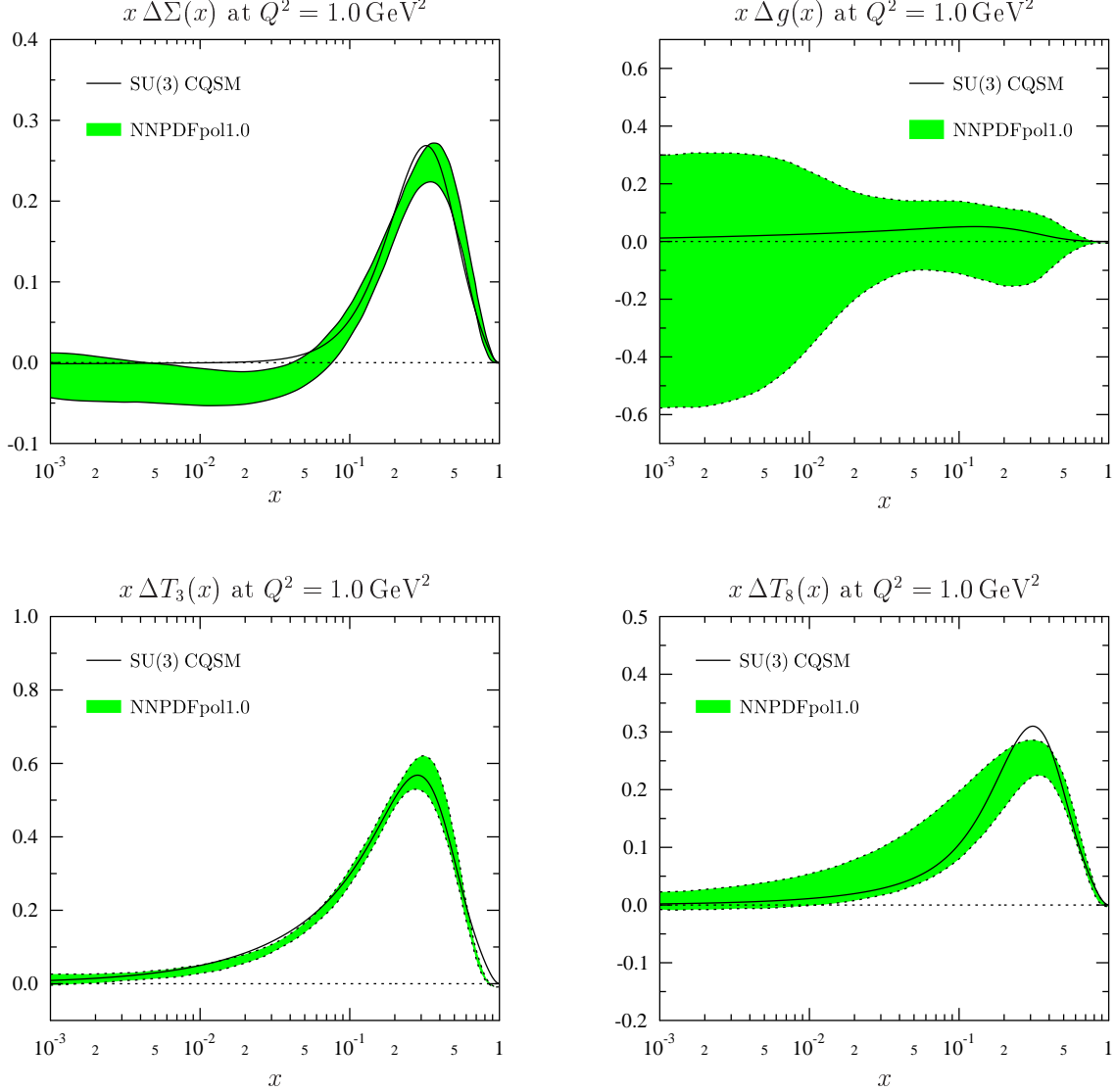


FIG. 11. The NNPDFpol1.0 fits for the polarized PDFs  $x \Delta T_3(x)$ ,  $x \Delta T_8(x)$ ,  $x \Delta \Sigma(x)$ , and  $x \Delta g(x)$  in comparison with the predictions of the SU(3) CQSM.

The Fig.11 shows the comparison for the polarized PDFs,  $x \Delta T_3(x)$ ,  $x \Delta T_8(x)$ ,  $x \Delta \Sigma(x)$ , and  $x \Delta g(x)$ . One can say that the agreement between the theoretical predictions and the global fits is fairly good, obviously much better than the case of the unpolarized PDFs.

From the similar analysis for the unpolarized distributions, we could have expected a good agreement for the non-singlet distributions like  $\Delta T_3(x)$  and  $\Delta T_8(x)$ . However, different from the unpolarized case, we clearly get much better agreement also for the flavor-singlet quark distribution  $\Delta\Sigma(x)$  and the gluon distribution  $\Delta g(x)$ . Remember that, in the case of unpolarized PDFs, the flavor singlet quark distribution was not reproduced very well. We argued that a possible reason of this discrepancy may be traced back to the neglect of the fact that the quark fields is likely to carry only about 80 % of the nucleon momentum at the model scale of  $Q_{ini}^2 \simeq 0.30 \text{ GeV}^2$ . Put another way, a good agreement for the flavor-singlet polarized distribution  $\Delta\Sigma(x)$  indicates that the neglect of the gluon contribution at the model energy scale does little harm. Accordingly, the following picture emerges. At the low energy scale corresponding to the CQSM, the gluon is likely to carry about 20 % of the nucleon momentum fraction, but it carries negligibly small polarization. It is interesting to point out that this observation is consistent with the claim in the paper by Efremov, Goeke, and Pobylitsa [101]. In fact, on the general ground of large  $N_c$  QCD, they argued that the polarized gluon distribution is  $1/N_c$  suppressed compared to the unpolarized one.

Note however that this does not mean that the gluon polarization remains to be small also at the high energy scales. If the quark has a positive polarization at the low energy scale, the polarization of gluon grows rapidly through the process of scale evolution. To get a feeling of the evolution effect, we solve the coupled evolution equation at the NLO for the net quark polarization and the gluon polarization at the NLO by starting with the initial condition of the CQSM, i.e.  $\Delta\Sigma = 0.35$  and  $\Delta G = 0.0$  at  $Q_{ini}^2 = 0.30 \text{ GeV}^2$ . The net gluon polarization  $\Delta G$  obtained in this way is shown in Table I for some typical values of  $Q^2$ .

TABLE I. The net longitudinal gluon polarization  $\Delta G$  in dependence of  $Q^2$ , obtained by solving the QCD evolution equation at the NLO under the assumption that  $\Delta G = 0$  and  $\Delta\Sigma = 0.35$  at the initial energy scale of the CQSM.

$Q^2$ [GeV <sup>2</sup> ]	0.30	1.0	4.0	10.0
$\Delta G(Q^2)$	0.0	0.21	0.40	0.51

We see that, even if we assume that  $\Delta G = 0$  at the low energy model scale, the gluon polarization increases rapidly as  $Q^2$  becomes large. Very recently, the DSSV collaboration

carried out a systematic analysis of the gluon polarization in the nucleon by paying particular attention to the data offered by polarized proton-proton collision available at the BNL Relativistic Heavy Ion Collider (RHIC) [102]. The final answer of their new global fit, corresponding to the scale  $Q^2 = 10 \text{ GeV}^2$ , is shown in Fig.5 of their paper. This figure give estimates for the 90 % C.L. area in the plane spanned by the truncated moments of  $\Delta g(x)$  calculated in  $0.05 \leq x \leq 1$  and  $0.001 \leq x \leq 0.05$ . Their result can be summarized as

$$\int_{0.05}^1 \Delta g(x) dx = 0.194 \begin{matrix} + 0.060 \\ - 0.060 \end{matrix} . \quad (12)$$

and

$$\int_{0.001}^{0.05} \Delta g(x) dx = 0.166 \begin{matrix} + 0.062 \\ - 0.046 \end{matrix} . \quad (13)$$

Summing up the contributions of both  $x$  region, this would give

$$\int_{0.001}^1 \Delta g(x) dx = 0.361 \begin{matrix} + 0.683 \\ - 0.522 \end{matrix} . \quad (14)$$

Note that the central value of the moment of  $\Delta g(x)$ , i.e.,  $\Delta G$  is positive with sizable magnitude, although the negative value is not completely excluded due to still large uncertainty coming from the integral in the small  $x$  region. It is clear from the analysis above that positive value of  $\Delta G$  is theoretically more than natural. If the result of global fits at high energy scale give negative gluon polarization, it would rather give us a puzzle, which is difficult to solve.

Next, in Fig.12, we compare the prediction of the SU(3) CQSM for the distributions  $x(\Delta u(x) + \Delta \bar{u}(x))$ ,  $x(\Delta d(x) + \Delta \bar{d}(x))$ ,  $x(\Delta s(x) + \Delta \bar{s}(x))$ , and also for  $x \Delta g(x)$  with the NNPDF fits together with a little older DSSV08 global fits. One sees that the model predictions for  $x(\Delta u(x) + \Delta \bar{u}(x))$  and  $x(\Delta d(x) + \Delta \bar{d}(x))$  are remarkably consistent with both of the NNPDF fits and the DSSV08 fits [103], which are close to each other, anyway. What is problematical is the polarized strange quark distribution. The NNPDF fit gives negative strange quark polarization, whereas the DSSV08 fit gives positive polarization at least in the larger  $x$  region. This means that the presently-available empirical information is not sufficient enough to determine the longitudinally polarized strange quark distribution with confidence. The difference between the two determinations lies in the fact that the DSSV fits depends more heavily on the data of semi-inclusive DIS reactions. As we have already

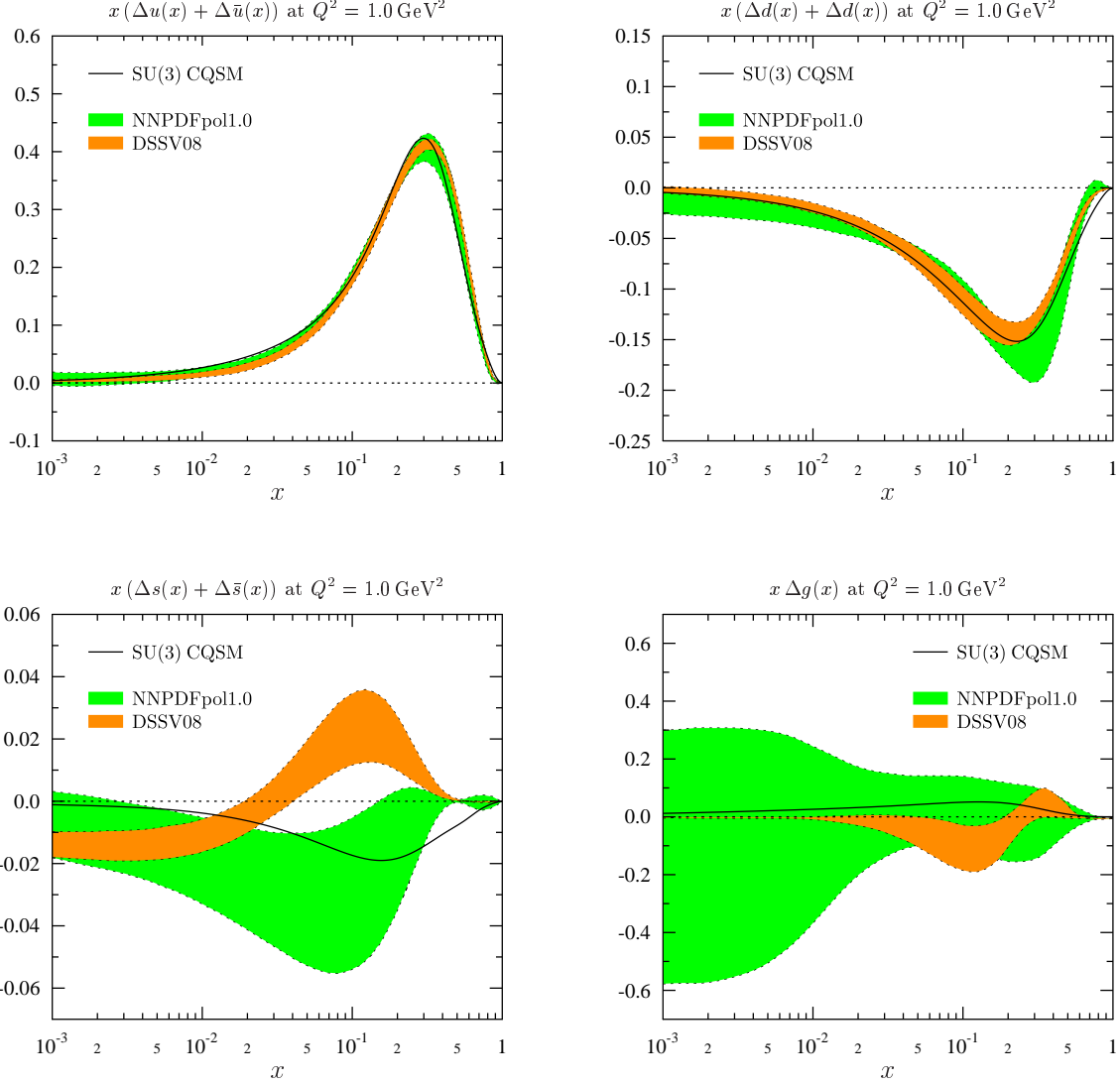


FIG. 12. The SU(3) CQSM predictions for the distributions  $x(\Delta u(x) + \Delta \bar{u}(x))$ ,  $x(\Delta d(x) + \Delta \bar{d}(x))$ ,  $x(\Delta s(x) + \Delta \bar{s}(x))$ , and also for  $x\Delta g(x)$  in comparison with the NNPDFpol1.0 fits [74] together with the DSSV08 fits [103].

pointed out, we feel that our understanding of the mechanism of the semi-inclusive reactions has not reached a satisfactory level as compared with the inclusive DIS reactions. At any rate, it is interesting to point out that the prediction of the SU(3) CQSM for the strange quark polarization is negative and consistent with the NNPDF fit at least qualitatively. Finally, the shapes of the gluon distributions are also fairly different between the NNPDF fit and the DSSV08 fit. However, the uncertainty bands for  $\Delta g(x)$  is sizably large in both fits. We point out that the prediction of the CQSM, obtained by assuming  $\Delta g(x) = 0$  at

the model scale, is within the (broad) error band of the NNPDF fit.

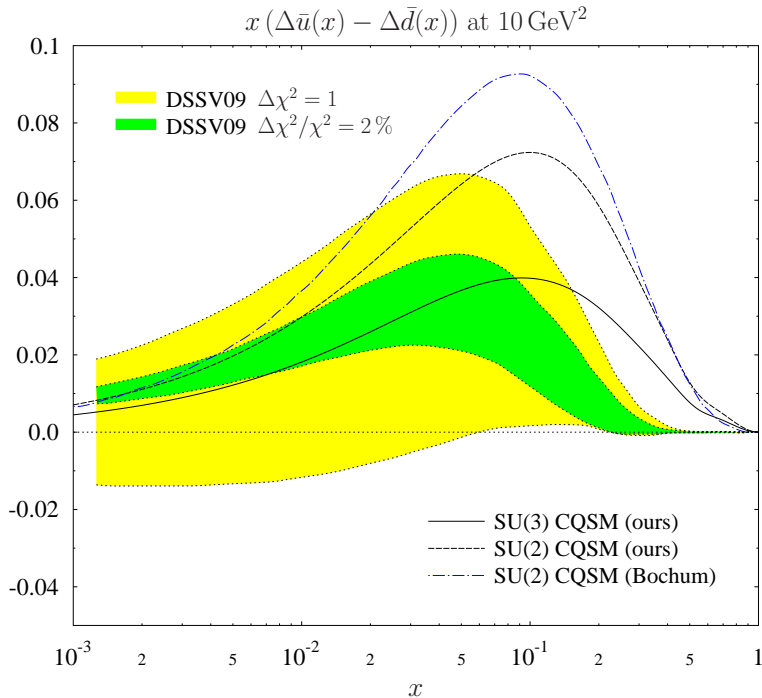


FIG. 13. The predictions of the SU(2) and SU(3) CQSM for the polarized light-flavor sea-quark asymmetry  $x(\Delta\bar{u}(x) - \Delta\bar{d}(x))$  in comparison with the DSSV09 global fit [104]. The dash-dotted curve is the prediction of the SU(2) CQSM by the Bochum group [105], whereas the long-dashed curve is our prediction in the same model. The prediction of the SU(3) CQSM is shown by the solid curve.

After confirming that the predictions of the SU(3) CQSM for the longitudinally polarized PDFs are remarkably consistent with the empirically extracted PDFs, especially the NNPDFpol1.0 fit, we now turn to more detailed inspection of the flavor structure of the longitudinally polarized sea-quark (anti-quark) distributions. We first show in Fig.13 the predictions of the CQSM for the flavor (or isospin) asymmetry for the longitudinally polarized sea-quark distributions, i.e.,  $x(\Delta\bar{u}(x) - \Delta\bar{d}(x))$  in comparison with the DSSV09 fit. The thinner (yellow in color) shaded area and the thicker (green in color) shaded area are the allowed bands of the DSSV09 fit given at  $Q^2 = 10 \text{ GeV}^2$ , respectively with  $\Delta\chi^2/\chi^2 = 2\%$  and with  $\Delta\chi^2 = 1$ . The solid curve is the prediction of the SU(3) CQSM, while the dashed curve is that of the SU(2) CQSM. The corresponding prediction of the Bochum group within the SU(2) CQSM is also shown for reference [105]. We first point out that our prediction and the that of Bochum group are sizably different in spite that they are the predictions

based on the same SU(2) CQSM. The reason of this discrepancy is not absolutely clear. We conjecture that a possible reason is that their calculation use schematic soliton profile function, while we use the solution of the self-consistent mean-field equation. Another reason may be that their predictions were obtained by using what-they-call the “interpolation formula”, which is an approximate method of calculating PDFs or any nucleon observables within the framework of the CQSM [43]. In any case, our prediction for  $\Delta\bar{u}(x) - \Delta\bar{d}(x)$  is significantly smaller than that of the Bochum group. Furthermore, the prediction of the SU(3) CQSM is much smaller than that of the SU(2) model. This provides a rare case in which the SU(3) CQSM and the SU(2) CQSM give a significantly different prediction for the light-flavor  $u$ - and  $d$ -quark distributions. One can see that the prediction of the SU(3) CQSM is order of magnitude consistent with the DSSV fit, although the positions of peak are slightly different. At any event, we find that the CQSM predicts fairly large flavor (isospin) asymmetry not only for the unpolarized sea-quark distributions but also for the longitudinally polarized sea-quark distributions. This should be contrasted with the prediction of the meson cloud models. Although it is known that the meson cloud models nicely reproduce the isospin asymmetry of the unpolarized sea-quark distributions, their predictions for the longitudinally polarized sea-quark distributions are generally very small or even diverging.

The reason why  $\Delta\bar{u}(x) - \Delta\bar{d}(x)$  is large was already discussed in several papers by Diakonov et al. [43],[44]. According to their large- $N_c$  argument,  $u(x) - d(x)$  and also  $\bar{u}(x) - \bar{d}(x)$  are  $1/N_c$  suppressed as compared with  $\Delta u(x) - \Delta d(x)$  and  $\Delta\bar{u}(x) - \Delta\bar{d}(x)$ , which was claimed to explain the fact that  $\Delta\bar{u}(x) - \Delta\bar{d}(x)$  is large. However, in reality  $N_c = 3$  and the explicit numerical calculation within the CQSM reveals that  $\bar{u}(x) - \bar{d}(x)$  and  $\Delta\bar{u}(x) - \Delta\bar{d}(x)$  actually have comparable magnitudes [52]. Furthermore, the large- $N_c$  argument tells us little about the  $x$ -dependencies of these distribution functions. The explicit  $x$ -dependencies can be known only through explicit numerical calculation within the CQSM. To answer the above question beyond the simple large- $N_c$  counting argument, we therefore think it instructive to look more closely at the predictions of the CQSM for four basic twist-2 PDFs, i.e. the isoscalar and isovector combinations of the unpolarized and longitudinally polarized PDFs. (To avoid inessential complexity, we show here the predictions of the SU(2) CQSM. This is enough because the essential physics of strong spin-isospin correlation is already embedded in the SU(2) model in the form of rotational symmetry-breaking mean-field.)

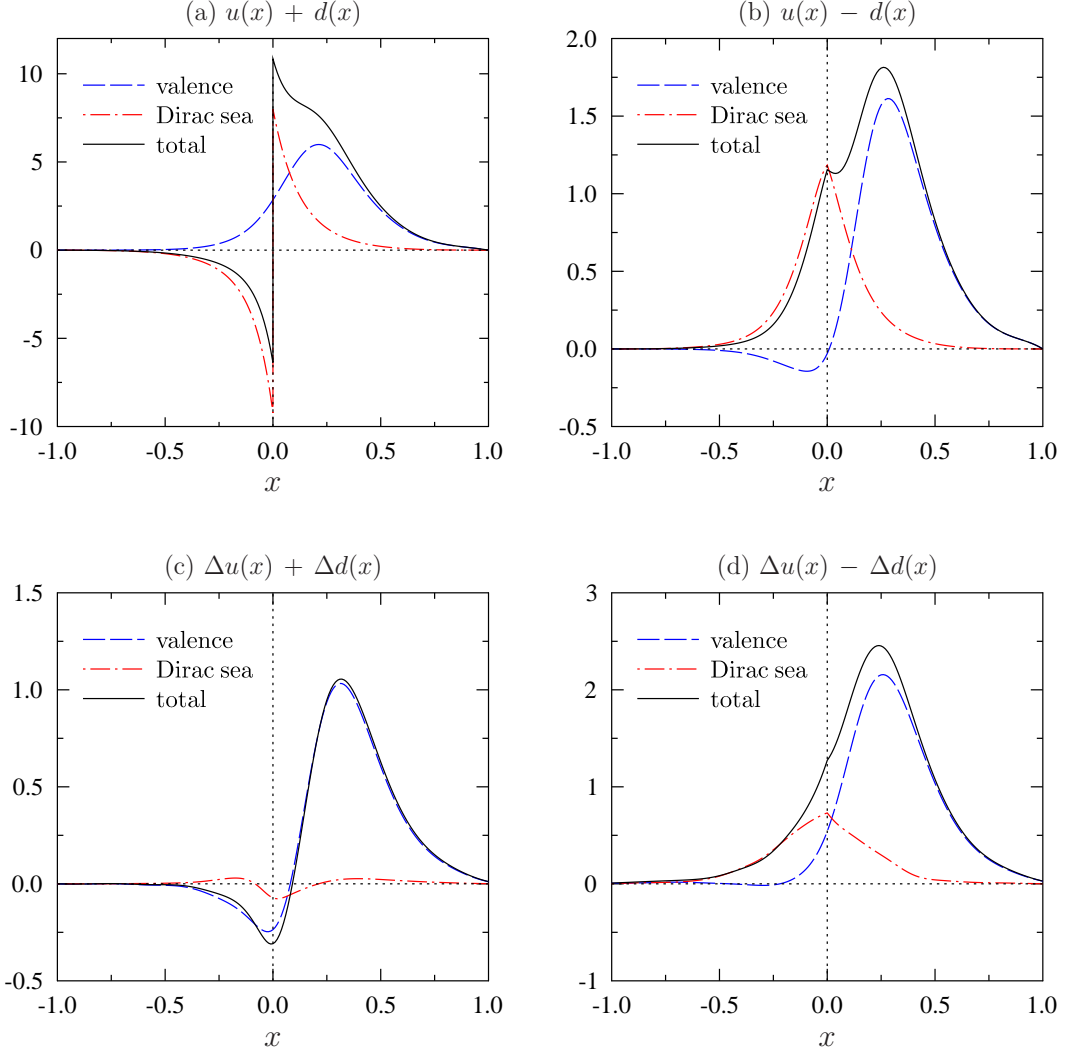


FIG. 14. The predictions of the SU(2) CQSM for the four basic twist-2 PDFs, i.e. the isoscalar and isovector combinations of the unpolarized and longitudinally polarized PDFs. In these figures, the long-dashed curves (blue in color) stand for the contributions of the three valence quarks in the mean field, whereas the dash-dotted curves (red in color) are those of the vacuum-polarized Dirac-sea quarks. The sums of these two contributions are shown by the solid curves.

In Fig.14, the long-dashed curves (blue in color) stand for the contributions of the three valence quarks in the mean field, whereas the dash-dotted curves (red in color) are those of the vacuum-polarized Dirac-sea quarks. The sums of these two contributions are shown by the solid curves. In these figures, the distribution functions in the negative  $x$  region must

be interpreted as antiquark distributions according to the rule :

$$u(-x) + d(-x) = -[\bar{u}(x) + \bar{d}(x)], \quad (15)$$

$$u(-x) - d(-x) = -[\bar{u}(x) - \bar{d}(x)], \quad (16)$$

$$\Delta u(-x) + \Delta d(-x) = +[\Delta \bar{u}(x) + \Delta \bar{d}(x)], \quad (17)$$

$$\Delta u(-x) - \Delta d(-x) = +[\Delta \bar{u}(x) - \Delta \bar{d}(x)], \quad (18)$$

with  $0 < x < 1$ . The sign-difference between the unpolarized and longitudinally polarized distributions originates from the symmetry properties of those under the charge-conjugation transformation. As one can see, the contributions of the three valence quarks have more or less similar shapes. They are peaked around  $x \sim (0.2 - 0.4)$ . On the other hand, one sees totally different behaviors of the contributions of Dirac-sea quarks in different distribution functions, all of which are already known to play important roles in reproducing the empirical distributions. One may however notice that the Dirac-sea contributions are surprisingly similar in shape for the two isovector distributions, i.e. for  $u(x) - d(x)$  and  $\Delta u(x) - \Delta d(x)$ . The fact that  $u(x) - d(x) > 0$  in the negative  $x$  region means  $\bar{u}(x) - \bar{d}(x) < 0$  for the physical value of  $x$  in the range  $0 < x < 1$ , which naturally explains the famous NMC observation. On the other hand,  $\Delta u(x) - \Delta d(x) > 0$  in the negative  $x$  region dictates that  $\Delta \bar{u}(x) - \Delta \bar{d}(x) > 0$  for physical  $x$ . We recall that, in the energy spectrum of the single-particle Dirac equation for quarks under the hedgehog mean field, there are two (deformed) Dirac continuums : the positive energy one and the negative energy one. Here, let us concentrate on the negative energy Dirac continuum and also on the Dirac-sea contribution to the PDFs in the negative  $x$  region, which correspond to antiquark distributions. The strong similarity in the shapes of  $u(x) - d(x)$  and  $\Delta u(x) - \Delta d(x)$  in the negative  $x$  region actually corresponds to anticorrelation, because of the rules (16) and (18). It appears that this anticorrelation is compatible with the grand spin zero nature of negative energy Dirac continuum, although more convincing argument is highly desirable. (We recall here the fact that the mean-field solution under the hedgehog potential is known to have a quantum number of  $K = 0$ , where  $\mathbf{K} \equiv \mathbf{S} + \mathbf{T}$ , with  $\mathbf{S}$  and  $\mathbf{T}$  being the ordinary spin and isospin operators, is called the grand spin operator.)

We have seen that the CQSM predicts large flavor asymmetry not only for the unpolarized sea-quark distribution but also for the longitudinally polarized sea-quark distribution, i.e.  $\Delta \bar{u}(x) - \Delta \bar{d}(x) > 0$ . Also interesting to know is separate information for polarized  $\bar{u}$  and

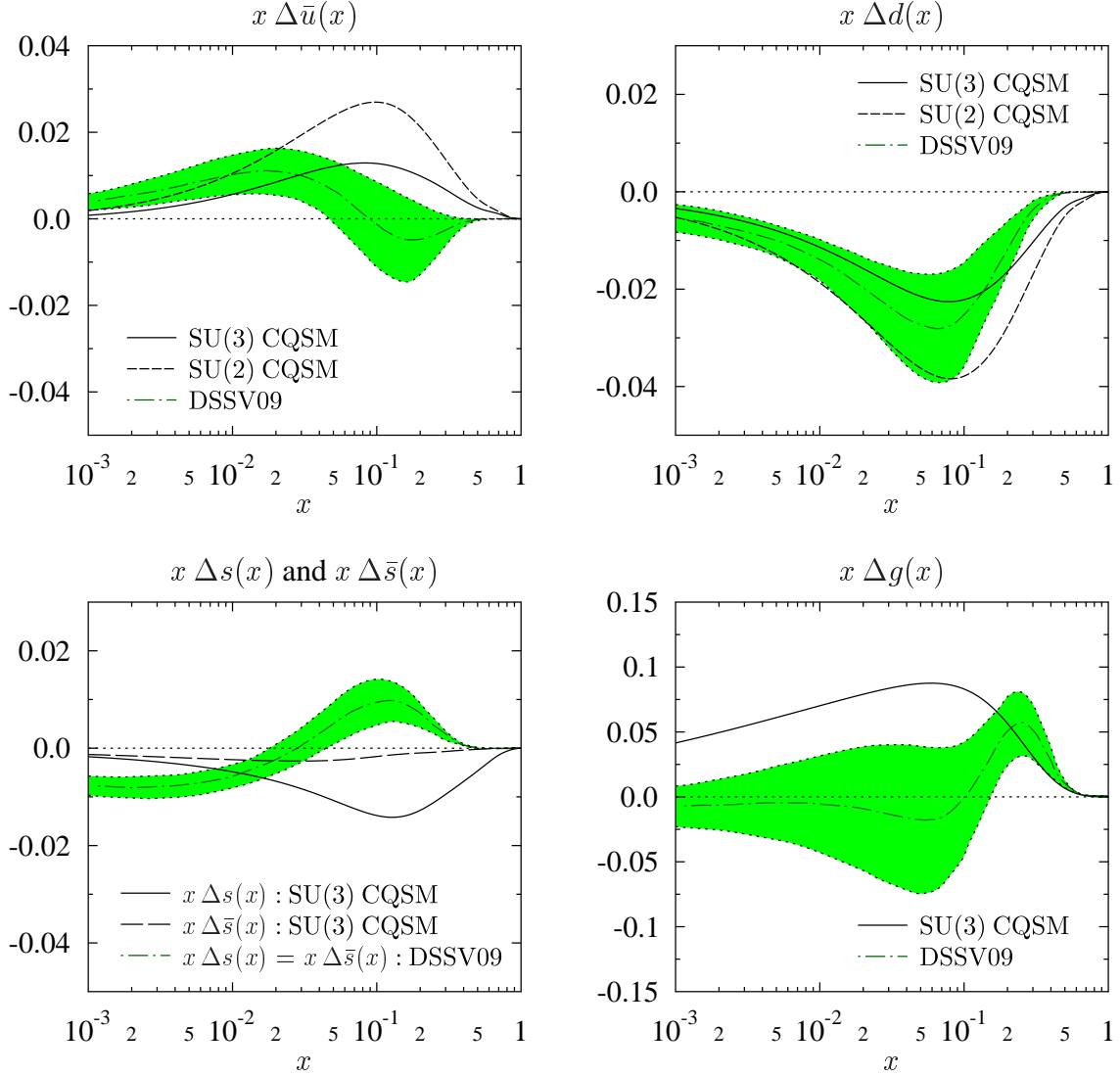


FIG. 15. The predictions of the SU(3) CQSM for the longitudinally polarized sea-quark distributions  $x\bar{u}(x)$ ,  $x\bar{d}(x)$ ,  $x\Delta s(x)$ ,  $x\bar{s}(x)$ , and the polarized gluon distribution  $\Delta g(x)$  evolved to  $Q^2 = 10 \text{ GeV}^2$  in comparison with the DSSV09 global fits [104].

$\bar{d}$  seas. Shown in Fig.15 are the predictions of the SU(3) CQSM in comparison with the DSSV09 fits [104]. For completeness, we also show a comparison for the polarized strange quark distribution and the polarized gluon distribution, because they are also given as a set in the DSSV09 fits. The model predicts that  $x\Delta\bar{u}(x)$  is positive, while  $x\Delta\bar{d}(x)$  is negative with sizable magnitude. One confirms that the predictions of the SU(3) CQSM for  $x\Delta\bar{u}(x)$  and for  $x\Delta\bar{d}(x)$  are both order of magnitude consistent with the DSSV09 fits. The DSSV central fit for the polarized  $\bar{u}$  distribution shows a nodal behavior around  $x \sim 0.08$ ,

which is not reproduced by the CQSM. From the theoretical viewpoint, however, such nodal behavior of the distribution  $\Delta\bar{u}(x)$  is difficult to understand. We again suspect that our incomplete understanding of the semi-inclusive processes can be a cause of this unnatural nodal behavior of the global fit. Turning to the strange quark distributions, the SU(3) CQSM predicts negative polarization, while the result of the DSSV09 fit is positive in the higher  $x$  range, where the distribution is dominant. However, we have already pointed out that the more recent NNPDF fits give negative strange quark polarization [74] in qualitatively consistent with the prediction of the SU(3) CQSM. Incidentally, in the DSSV analysis, the equality of the polarized strange and anti-strange distributions are assumed from the beginning. Very interestingly, according to the SU(3) CQSM, the negative polarization of the strange plus anti-strange distribution turns out to mostly come from the strange quark and the polarization of the anti-strange quark is very small. This means that the model predicts sizable particle-antiparticle asymmetry not only for the unpolarized strange quark distributions but also for the longitudinally polarized ones. We recall that this feature is also qualitatively consistent with the picture of the kaon cloud model proposed by Signal and Thomas [58], Burkardt and Warr [59], and also by Brodsky and Ma [60]. In fact, the strange sea in the proton is thought to be generated through the virtual dissociation process of the proton into the  $\Lambda$  and the  $K^+$ , i.e.  $p \rightarrow \Lambda + K^+$ . Note an apparent asymmetry of the  $s$ -quark and  $\bar{s}$ -quark in this process. The  $s$ -quark is contained in the spin one-half  $\Lambda$ , while the  $\bar{s}$ -quark is contained in the spin zero  $K^+$ . This naturally explains the reason why the polarization of  $\bar{s}$ -quark is smaller than that of  $s$ -quark.

#### IV. FLAVOR SU(3) CQSM AND CHARGE-SYMMETRY-VIOLATING PDFS

The effective lagrangian, which takes account of the charge-symmetry-violation (CSV), is given as

$$\mathcal{L} = \mathcal{L}_0 + \mathcal{L}_{SB} + \mathcal{L}_{CSV}, \quad (19)$$

where  $\mathcal{L}_0$  and  $\mathcal{L}_{SB}$  were already given, while the CSV part  $\mathcal{L}_{CSV}$  can be written as

$$\mathcal{L} = -\Delta m \bar{\psi} \frac{\lambda_3}{2} \psi, \quad (20)$$

with  $\Delta m \equiv m_u - m_d \simeq -4$  MeV. The CSV effects for the PFDs in the nucleon can be investigated by treating this SU(2) breaking part of the effective lagrangian as the first order

perturbation. The general method is exactly the same as the one used in the perturbative treatment of the SU(3) symmetry breaking term  $\mathcal{L}_{SB}$ . Note however mass difference between the  $u$  and  $d$  quarks is far smaller than that between the strange quark and the  $u, d$  quarks. Consequently, the perturbative treatment of the CSV part  $\mathcal{L}_{CSV}$  has even better foundation than that of  $\mathcal{L}_{SB}$ . Since the necessary formalism is already explained in our previous paper, we do not repeat the detailed derivation here. For completeness, however, we just summarize below the final theoretical expressions, which are necessary for the actual calculation.

Within the framework of the SU(3) CQSM, the PDFs for the  $u, d, s$  quarks are represented as linear combinations of three independent functions  $q^{(0)}(x)$ ,  $q^{(3)}(x)$ , and  $q^{(8)}(x)$  as

$$u(x) = \frac{1}{3}q^{(0)}(x) + \frac{1}{2}q^{(3)}(x) + \frac{1}{2\sqrt{3}}q^{(8)}(x), \quad (21)$$

$$d(x) = \frac{1}{3}q^{(0)}(x) - \frac{1}{2}q^{(3)}(x) + \frac{1}{2\sqrt{3}}q^{(8)}(x), \quad (22)$$

$$s(x) = \frac{1}{3}q^{(0)}(x) - \frac{1}{\sqrt{3}}q^{(8)}(x). \quad (23)$$

In the SU(3) symmetric limit, these three distributions generally consist of the zeroth order term and the first order term in the corrective angular velocity  $\Omega$  of the rotating soliton. (The zeroth order term corresponds to the mean-field predictions.) They are given in the form :

$$q^{(0)}(x) = \langle 1 \rangle_N \cdot f(x), \quad (24)$$

$$q^{(3)}(x) = \left\langle \frac{D_{38}}{\sqrt{3}} \right\rangle_N \cdot f(x) + \left\langle \sum_{i=1}^3 \{D_{3i}, R_i\} \right\rangle_N \cdot k_1(x) + \left\langle \sum_{K=4}^7 \{D_{3K}, R_K\} \right\rangle_N \cdot k_2(x) \quad (25)$$

$$q^{(8)}(x) = \left\langle \frac{D_{88}}{\sqrt{3}} \right\rangle \cdot f(x) + \left\langle \sum_{i=1}^3 \{D_{8i}, R_i\} \right\rangle_N \cdot k_1(x) + \left\langle \sum_{K=4}^7 \{D_{8K}, R_K\} \right\rangle_N \cdot k_2(x). \quad (26)$$

The functions  $f(x)$ ,  $k_1(x)$ , and  $k_2(x)$  are defined in Eqs.(33), (76), and (77) of the paper [53]. (They are all calculable, once the solutions of the mean-field equations are given.) Here, the terms containing the function  $f(x)$  is the zeroth order term in  $\Omega$ , while the terms containing the functions  $k_1(x)$  and  $k_2(x)$  are the 1st order terms in  $\Omega$ . The  $D_{ab}$ 's as functions of the collective coordinates  $\xi_A$  are the standard Wigner rotation matrices, while  $R_a$  is the right rotation generator familiar in the SU(3) Skyrme model. In the above expressions,

$\langle O \rangle_B$  should be understood as an abbreviated notation of the matrix element of a collective operator  $O$  between a baryon state  $B$  with appropriate quantum numbers, i.e.

$$\langle O \rangle_B \equiv \int \Psi_{YTT_3;JJ_3}^{(n)*}[\xi_A] O[\xi_A] \Psi_{YTT_3;JJ_3}^{(n)}[\xi_A] d\xi_A. \quad (27)$$

The relevant matrix elements of the collective space operators between the nucleon state, appearing in the above expressions, are already given in Eqs.(186)-(188) of the paper [53].

There are two types of CSV corrections to the distributions,  $q^{(0)}(x)$ ,  $q^{(3)}(x)$ , and  $q^{(8)}(x)$ . We can show that the first corrections, which were called the dynamical plus kinematical corrections in [53] (see also [106],[107]), are given by

$$q^{(0)}(x; \Delta m^{dyn+kin}) = -\frac{2\Delta m I_1}{\sqrt{3}} \langle D_{38} \rangle_N \cdot \tilde{k}_0(x), \quad (28)$$

$$\begin{aligned} q^{(3)}(x; \Delta m^{dyn+kin}) &= -\frac{2\Delta m_s I_1}{3} \langle D_{38} D_{38} \rangle_N \cdot \tilde{k}_0(x) \\ &\quad - \Delta m I_1 \left\langle \sum_{i=1}^3 \{D_{38}, D_{38}\} \right\rangle_N \cdot \left[ \tilde{k}_1(x) - \frac{K_1}{I_1} k_1(x) \right] \\ &\quad - \Delta m I_2 \left\langle \sum_{i=4}^7 \{D_{3K}, D_{3K}\} \right\rangle_N \cdot \left[ \tilde{k}_2(x) - \frac{K_2}{I_2} k_2(x) \right], \quad (29) \end{aligned}$$

$$\begin{aligned} q^{(8)}(x; \Delta m^{dyn+kin}) &= -\frac{2\Delta m I_1}{3} \langle D_{88} D_{88} \rangle_N \cdot \tilde{k}_0(x) \\ &\quad - \Delta m I_1 \left\langle \sum_{i=1}^3 \{D_{8i}, D_{3i}\} \right\rangle_N \cdot \left[ \tilde{k}_1(x) - \frac{K_1}{I_1} k_1(x) \right] \\ &\quad - \Delta m I_2 \left\langle \sum_{i=4}^7 \{D_{8K}, D_{3K}\} \right\rangle_N \cdot \left[ \tilde{k}_2(x) - \frac{K_2}{I_2} k_2(x) \right]. \quad (30) \end{aligned}$$

Here,  $I_1$ ,  $I_2$ ,  $K_1$ , and  $K_2$  are various moments of inertia of the soliton defined through Eqs.(49)-(52) in the paper [53]. On the other hand, the functions  $\tilde{k}_0(x)$ ,  $\tilde{k}_1(x)$  and  $\tilde{k}_2(x)$  are respectively given in Eqs.(142), (155), and (156) in the same paper [53].

The necessary matrix elements of the collective space operators between the proton state can easily be calculated and they are shown in Table II. The three matrix elements in the left column take the same values also for the neutron state, whereas the four matrix elements in the right column changes signs for the neutron state.

The second correction to the PDFs arises from the mixing of the SU(3) representation by the CSV mass term [53],[106],[107]. Due to the presence of the CSV mass term, the nucleon state is not a pure SU(3) octet, but it is a linear combination of three SU(3) representation

TABLE II. The matrix elements of the relevant collective space operators in the proton state.

—	$\left\langle \frac{D_{38}}{\sqrt{3}} \right\rangle_p = \frac{1}{30}$
$\langle D_{38} D_{38} \rangle_p = \frac{1}{15}$	$\langle D_{88} D_{38} \rangle_p = 0$
$\left\langle \sum_{i=1}^3 \{D_{3i}, D_{3i}\} \right\rangle_p = \frac{10}{9}$	$\left\langle \sum_{i=1}^3 \{D_{8i}, D_{3i}\} \right\rangle_p = \frac{2\sqrt{3}}{45}$
$\left\langle \sum_{K=4}^7 \{D_{3K}, D_{3K}\} \right\rangle_p = \frac{34}{45}$	$\left\langle \sum_{K=1}^3 \{D_{8K}, D_{3K}\} \right\rangle_p = -\frac{2\sqrt{3}}{45}$

as

$$|N\rangle \simeq |8, N\rangle + d_{10}^N |\bar{10}, N\rangle + d_{27}^N |27, N\rangle, \quad (31)$$

with the mixture constants,

$$d_{10}^N = \frac{\sqrt{5}}{15} \left( \alpha' + \frac{1}{2} \gamma' \right) I_2, \quad (32)$$

$$d_{27}^N = -\frac{\sqrt{6}}{75} \left( \alpha' - \frac{1}{6} \gamma' \right) I_2. \quad (33)$$

Here, the constants  $\alpha'$  and  $\gamma'$  are given by

$$\alpha' = \left( \frac{\bar{\sigma}}{N_c} - \frac{K_2}{I_2} \right) \frac{\Delta m}{2}, \quad (34)$$

$$\gamma' = - \left( \frac{K_1}{I_1} - \frac{K_2}{I_2} \right) \Delta, \quad (35)$$

with  $N_c = 3$  being the number of colors, whereas  $\bar{\sigma}$  is defined in Eq.(206) of [53].

Putting all the functions above together, the CSV corrections to the PDFs can be evaluated in the following manner :

$$\begin{aligned} \delta u(x) \equiv u^p(x) - d^n(x) &= \frac{2}{3} \delta q^{(0)}(x; \Delta m^{dyn+kin}) \\ &+ [\delta q^{(3)}(x; \Delta m^{dyn+kin}) + \delta q^{(3)}(x; \Delta m^{rep})] \\ &+ \frac{1}{\sqrt{3}} [\delta q^{(8)}(x; \Delta m^{dyn+kin}) + \delta q^{(8)}(x; \Delta m^{rep})], \end{aligned} \quad (36)$$

$$\begin{aligned} \delta d(x) \equiv d^p(x) - u^n(x) &= \frac{2}{3} \delta q^{(0)}(x; \Delta m^{dyn+kin}) \\ &- [\delta q^{(3)}(x; \Delta m^{dyn+kin}) + \delta q^{(3)}(x; \Delta m^{rep})] \\ &+ \frac{1}{\sqrt{3}} [\delta q^{(8)}(x; \Delta m^{dyn+kin}) + \delta q^{(8)}(x; \Delta m^{rep})], \end{aligned} \quad (37)$$

$$\begin{aligned} \delta s(x) \equiv s^p(x) - s^n(x) &= \frac{2}{3} \delta q^{(0)}(x; \Delta m^{dyn+kin}) \\ &- \frac{2}{\sqrt{3}} [\delta q^{(8)}(x; \Delta m^{dyn+kin}) + \delta q^{(8)}(x; \Delta m^{rep})]. \end{aligned} \quad (38)$$

Now, we show in Fig.16 the predictions of the SU(3) CQSM for the CSV PDFs evolved to the scale  $Q^2 = 10 \text{ GeV}^2$  in comparison with some other theoretical predictions. The solid and long-dashed curves (black in color) respectively stand for the predictions of the SU(3) CQSM for  $x \delta u_V \equiv x [u_V^p(x) - d_V^n(x)]$  and  $x \delta d_V \equiv x [d_V^p(x) - u_V^n(x)]$ . The long dash-dotted and dotted curves (red in color) are the predictions of Rodionov, Thomas, and Londergan based on the bag model with quark-diquark correlations [68]. On the other hand, the short-dashed and short dash-dotted (blue in color) are the predictions of Glück, Jimenez-Delgado, and Reya based on the QED radiative (or splitting) mechanism [70]. (The CSV effects arising from the QED splitting mechanism was also proposed by Martin et al. independently [71].

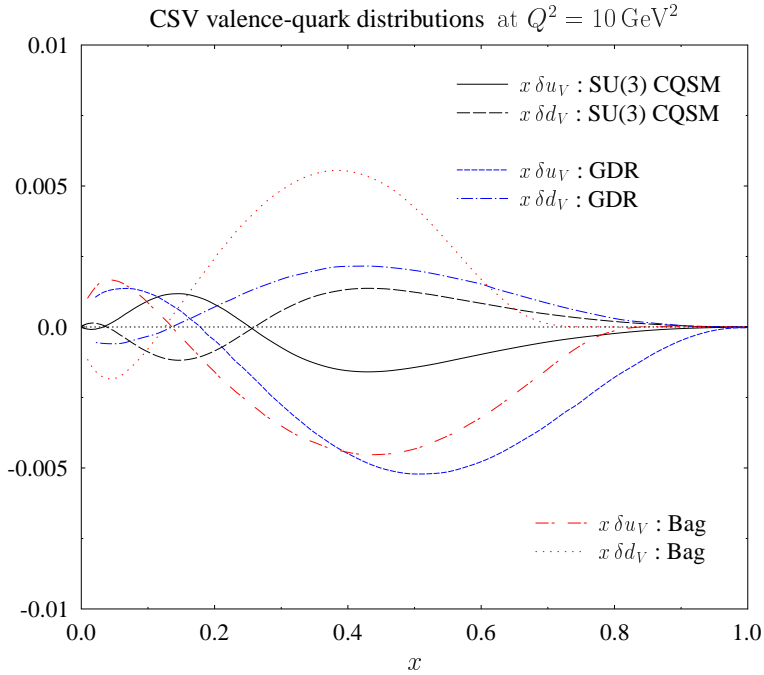


FIG. 16. The predictions of the SU(3) CQSM for the CSV PDFs  $\delta u_V(x)$  and  $\delta d_V(x)$  corresponding  $Q^2 = 10 \text{ GeV}^2$ . Also shown are the bag model predictions by Rodionov, Thomas, and Londergan [68], and the predictions based on the QED radiative mechanism by Glück et al. [70]

First, we point out that all the models predicts that  $\delta u_V(x) < 0$  and  $\delta d_V(x) > 0$  at least for the dominant components in the larger  $x$  region. Comparing the predictions of the SU(3) CQSM and those of the bag model, we find that the former are much smaller than the latter. To understand the cause of this difference, it is instructive to compare the basic framework of these models in some detail. In the framework of the CQSM, the mass

difference between the  $u$ - and  $d$ -quarks is the only origin of the CSV effects in the PDFs. Once the perturbative treatment of this mass difference is accepted, there is no ambiguity in the theoretical treatment. On the other hand, refined bag model treatment of Rodionov et al. is based on quite a different assumption on the CSV mechanism [68], which was first proposed by Sather [67] and has been used in most investigations of the CSV PDFs in the past. This treatment is critically dependent on the quark-diquark picture for the intermediate states in the DIS amplitudes. To be more concrete, their treatment starts with the parton model expression for a quark distribution function given as

$$q(x) = M_N \sum_X |\langle X | \psi_+(0) | N \rangle|^2 \times \delta(M_N(1-x) - p_X^+), \quad (39)$$

where  $\psi_{\pm} = (1 + \gamma^0 \gamma^3) \psi / 2$ , while  $|N\rangle$  is the nucleon state, while  $|X\rangle$  is all possible final state, which is obtained from  $|N\rangle$  by removing a quark or adding an antiquark. The state  $|X\rangle$  is thought to have the following Fock-space expansion,  $|X\rangle = 2q, 3q + \bar{q}, 4q + 2\bar{q}, \dots$ . Based on the idea that, for large enough  $x$ , say,  $x \geq 0.2$ , the valence quarks dominate, it is postulated that a reasonable estimate of  $q(x)$  can be obtained by including only two-quark intermediate states for  $|X\rangle$ . It is further assumed that this intermediate two-quark state can be approximated by a diquark with definite mass  $M_D$ . The validity of both these assumptions is not absolutely clear. Especially, the latter postulate, i.e. the two-body kinematics in the intermediate state, is a highly nontrivial assumption. We refer to the paper [108] by Cao and Signal for the detailed criticism to the framework of evaluating the CSV effects in PDFs based on the quark-diquark hypothesis.

In any case, a common feature of most calculations based on this quark-diquark picture is that they predict fairly large CSV corrections in PDFs ranging from 2% to 10%, which is much larger than the CSV effects expected from the low energy CSV phenomena, which are generally known to be less than 1%. In view of this situation, it is important to estimate the size of CSV effects in PDFs without relying upon the quark-diquark picture. So far, there have been only a few such attempts. The one is the study by Cao and Signal based on a meson cloud model [108]. In their treatment, hadron mass differences between the isospin multiplets are the only sources of the CSV effects in PDFs. Another independent analysis was carried out by Benesh and Goldman based on a quark model [109]. In their treatment, the effects due to the  $u$ - $d$  quark mass difference and the Coulomb interaction of the electrically charged quarks are taken into account. Both of these studies shows that

the CSV effects in PDFs are considerably smaller than those obtained based on the quark-diquark picture. The present calculation based on a totally different theoretical framework appears to give another support to this conclusion by Cao and Signal and also by Benesh and Goldman.

Since our main purpose of investigating the CSV PDFs is to get a feeling about the relative importance the CSV effects and the asymmetry of the strange and antistrange quark distributions in the resolution scenario of the NuTeV anomaly, we compare these distributions in Fig.17. Here, the solid curve is the bare prediction of the CQSM for  $x [s(x) - \bar{s}(x)]$ , while the long-dashed curve is the reduced prediction by a factor of 1/2. (The latter is our favorable prediction, as explained before.) The dash-dotted curve (red in color) is the CQSM prediction for the CSV valence distribution  $x [\delta u_V(x) - \delta d_V(x)]$  divided by a factor of 2. (Compare Eq.(41) and Eq.(42) below for the reason why we divide it by 2.) One sees that the CSV valence quark distribution is much smaller than the asymmetry of strange and antistrange quark distribution calculated within exactly the same theoretical framework.

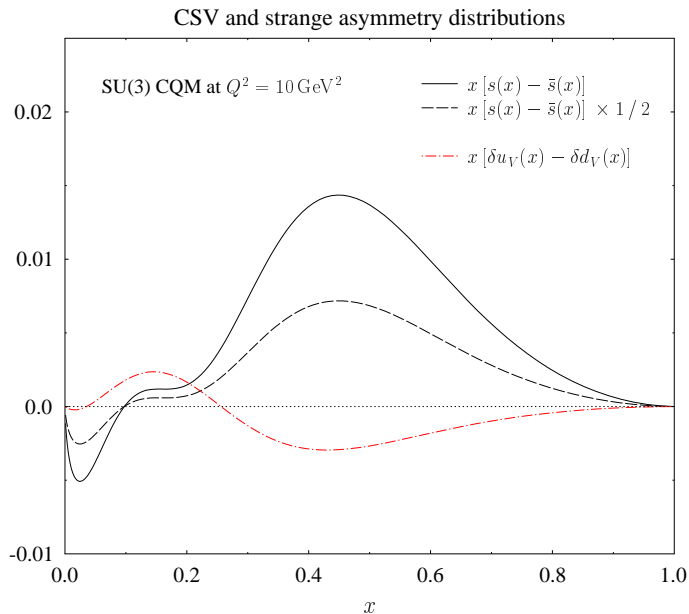


FIG. 17. The SU(3) CQM predictions for the CSV valence quark distribution in comparison with the strange asymmetry distribution.

As is well-known, the main QCD correction to the Paschos-Wolfenstein ration is approx-

imately given by the following formula :

$$R^- \equiv \frac{\sigma_{NC}^{\nu N} - \sigma_{NC}^{\bar{\nu} N}}{\sigma_{CC}^{\nu N} - \sigma_{CC}^{\bar{\nu} N}} = R_{PW}^- + \delta R_I^- + \delta R_s^-, \quad (40)$$

where

$$\delta R_I^- \simeq \left(1 - \frac{7}{3} s_W^2\right) \frac{\delta U_V - \delta D_V}{2(U_V + D_V)}, \quad (41)$$

$$\delta R_s^- \simeq - \left(1 - \frac{7}{3} s_W^2\right) \frac{S^-}{U_V + D_V}, \quad (42)$$

with  $s_W^2 \equiv \sin^2 \theta_W = 0.2227 \pm 0.0004$  and

$$Q_V(Q^2) = \int_0^1 x q_V(x, Q^2) dx \quad (43)$$

$$\delta Q_V(Q^2) = \int_0^1 x \delta q_V(x, Q^2) dx, \quad (44)$$

$$S^-(Q^2) = \int_0^1 x [s(x, Q^2) - \bar{s}(x, Q^2)] dx. \quad (45)$$

Glück et al. [70] as well as the NuTeV group [56],[57] pointed out that the above approximate formula is not accurate enough and proposed more refined formula to determine the CSV effects on the determination of  $\sin \theta_W$ . However, since our main interest here is the relative importance of the CSV effects and the particle-antiparticle asymmetry of the strange quark distribution, we use the above formula below. Using the obtained distributions corresponding to the scale  $Q^2 = 10 \text{ GeV}^2$ , we get the following estimate for the CSV correction of QCD origin :

$$\Delta s_W^2|_{CSV} \simeq \delta R_I^-|_{QCD} \simeq -0.00035. \quad (46)$$

On the other hand, the correction due to the strange-antistrange asymmetry is given by

$$\Delta s_W^2|_{strange} \simeq \delta R_s^- = -0.00264 (-0.00528). \quad (47)$$

Here, the number in the parenthesis is the bare prediction of the SU(3) CQSM not being multiplied by a reduced factor of 1/2. Note that this estimate is order of magnitude consistent with the independent estimate by Ding, Xu, and Ma [64], which gives  $\delta R_s^- \simeq -(0.00297 - 0.00498)$ . One confirms that the effect of CSV originating from the  $u-d$  quark mass difference is order of magnitude smaller than that of the strange asymmetry. We however recall that there is another mechanism which generate the CSV effects in the

quark distributions. It is the QED splitting mechanism proposed by Glück et al. and also by Martin et al. The recent estimate by Glück et al. gives

$$\Delta s_W^2|_{QED} = \delta R_I^-|_{QED} = -0.002. \quad (48)$$

Since this CSV mechanism is of QED origin and it is totally independent of the CSV effect of QCD origin, we may add all the above corrections to the Weinberg angle. This gives

$$\begin{aligned} \Delta s_W^2|_{sum} &= \text{QED} + \text{Strange} + \text{CSV} \\ &= -0.002 - 0.00264 - 0.00035 \\ &\simeq -0.0050. \end{aligned} \quad (49)$$

This means that the NuTeV measurement of  $\sin^2 \theta_W = 0.2277(16)$  will be shifted to  $\sin^2 \theta_W = 0.2227(16)$  which agree with the standard value  $0.2228(4)$ , although we should perform more careful analysis in view of the approximate nature of the above correction formula. Anyhow, our finding here can be summarized as follows. The effect of the particle-antiparticle asymmetry of the strange quark distribution to the NuTeV anomaly seems to be much larger than the CSV effect in the valence quark distribution originating from the  $u$ - $d$  quark mass difference. However, the CSV effect due to the QED splitting mechanism is an increasing function of the scale [70],[71] and its effect on the NuTeV anomaly can have the same order of magnitude as that of the strange asymmetry at the scale of  $Q^2 = 10 \text{ GeV}^2$ .

Since one of the advantages of the CQSM is that it can give reasonable predictions not only for the quark distributions but also for the antiquark distributions, we think it interesting to evaluate the CSV effect in the sea-quark distributions in this model. The solid and long-dashed curves in Fig.18 represent the CSV light-flavor sea-quark distributions defined by

$$\delta \bar{u}(x) \equiv \bar{u}^p(x) - \bar{d}^n(x), \quad (50)$$

$$\delta \bar{d}(x) \equiv \bar{d}^p(x) - \bar{u}^n(x). \quad (51)$$

Here, the solid and long-dashed curves (black in color) correspond to the predictions of the SU(3) CQSM, while the dash-dotted and short-dashed curves (blue in color) correspond to the predictions based on the QED splitting mechanism [70]. Very curiously, the predictions of the SU(3) CQSM for  $\delta \bar{u}(x)$  and  $\delta \bar{d}(x)$  and the corresponding predictions due to the QED

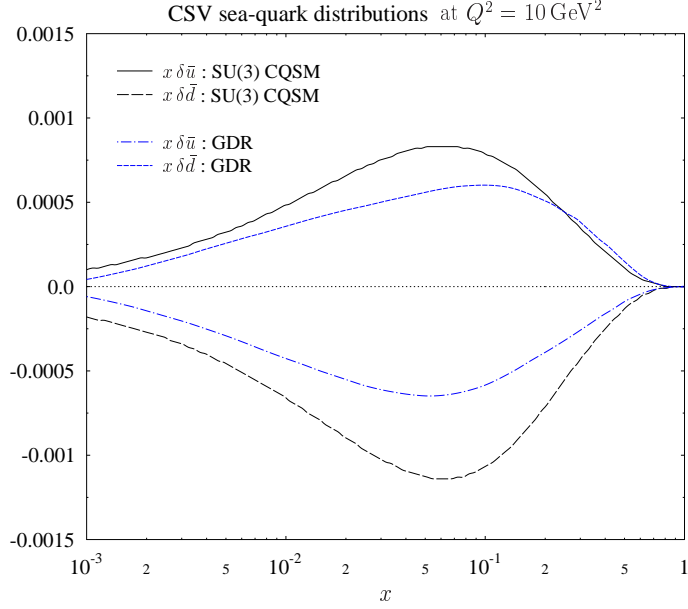


FIG. 18. The predictions of the SU(3) CQSM for the CSV sea-quark (antiquark) distributions at  $Q^2 = 10 \text{ GeV}^2$  in comparison with the corresponding distributions generated by the QED splitting mechanism [70].

splitting mechanism have nearly equal magnitudes but their signs are opposite. This means that, if we add up both contributions, a sizable cancellation occurs, which would indicate that the net CSV effects on the sea-quark distribution would be very small and hard to observe experimentally.

Finally, just to make sure, we estimate the CSV effect on the valence-like strange quark distribution, i.e.  $s^-(x) \equiv s(x) - \bar{s}(x)$  in comparison with the CSV effects on the light-flavor valence quark distribution. The results are shown in Fig.19. One simply confirms that the CSV effect on the strange distribution is in fact very small.

## V. SUMMARY AND CONCLUSION

To conclude, we have analyzed the unpolarized and the longitudinally polarized PDFs in the nucleon within a single theoretical framework of the SU(3) CQSM, which contains only one adjustable parameter  $\Delta m_s$ , the mass difference between the strange and nonstrange quarks. Through detailed comparisons with the recent global PDF fits by the NNPDF

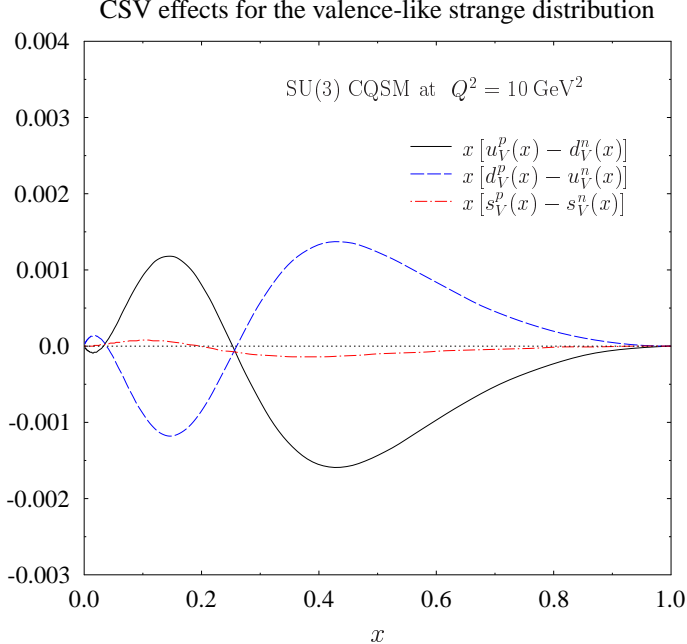


FIG. 19. The SU(3) CQSM prediction for the CSV effects to the valence-like strange quark distribution  $x [s_V^p(x) - s_V^n(x)]$  with  $s_V(x) \equiv s(x) - \bar{s}(x)$  in comparison with the CSV effects to the light-flavor valence-like distributions  $x [u_V^p(x) - d_V^n(x)]$  and  $x [d_V^p(x) - u_V^n(x)]$ .

group, the DSSV group, and the CTEQ group, etc., we could confirm that, despite its nearly parameter-free nature, the model reproduces all the qualitative characteristics of the empirically determined PDFs. Besides, it gives unique and nontrivial predictions on the flavor structure of the sea-quark distributions. They are the flavor asymmetry of the unpolarized sea-quark distributions,  $\bar{u}(x) - \bar{d}(x) < 0$ , dictated by the famous NMC measurement, the flavor asymmetry of the longitudinally polarized sea-quark distributions,  $\Delta\bar{u}(x) > 0$ ,  $\Delta\bar{d}(x) < 0$ , the particle-antiparticle asymmetry of the unpolarized strange quark distribution,  $s(x) - \bar{s}(x) \neq 0$ , and also the particle-antiparticle asymmetry of the longitudinally polarized strange quark distributions,  $\Delta s(x) < 0$ ,  $\Delta\bar{s}(x) \simeq 0$ . The success is naturally connected with the fact that the model incorporates the most important feature of the QCD in the nonperturbative low energy domain, i.e. the spontaneous chiral symmetry breaking and the appearance of the associated Goldstone bosons. Still, an important difference with more familiar meson cloud models should be clearly recognized. As stated above, the CQSM predicts large isospin asymmetry not only for the unpolarized seas but also for the longitudinally polarized ones. On the other hand, although the meson cloud models nicely explains

the flavor asymmetry of the unpolarized sea-quark distributions, they generally predict very small spin polarization of sea quarks, reflecting the fact that the pion carries no spin and the effects of heavier meson cloud are suppressed. In view of this important difference, more unambiguous confirmation of the flavor asymmetry of the longitudinally polarized sea-quark distribution is an urgent task.

We have pointed out that, for that the model predictions are taken as reliable also in a quantitative sense, we need two remedies. First, the information from phenomenological global fits indicates that the gluon carries about 20 % of the nucleon momentum fraction even at the low energy scale corresponding to the CQSM. Naturally, this fact is not properly incorporated in effective quark models like the CQSM. As we have seen, this seems to be a cause of about 20 % overestimate of the flavor-singlet combination of the unpolarized PDFs. However, we have also shown that the neglect of the gluon degrees of freedom at the model energy scale is likely to do little harm in the case of the longitudinally polarized PDFs. This is the reason why the success of the model is more salient for the longitudinally polarized PDFs than for the unpolarized PDFs. The second problem is that the SU(3) symmetric collective quantization (with the subsequent perturbative treatment of the SU(3) symmetry breaking mass difference between the strange and nonstrange quarks) might tend to overestimate the kaon cloud effects, thereby having a danger of overvaluing the magnitudes of the strange quark distributions. As the present analysis, especially the detailed comparison with the unbiased NNPDF global fits, strongly indicates, plausible predictions for the strange and antistrange quark distributions would correspond to an average of the SU(3) and SU(2) CQSM, which means that we can get reliable predictions for the strangeness-related distributions if we multiply a reduction factor of about 1/2 to the bare predictions of the SU(3) CQSM. After this modification to the strange quark distributions is taken into account, we have good reason to believe that the SU(3) CQSM is already giving reliable predictions with (20 – 30)% accuracy for both of the unpolarized and longitudinally polarized PDFs, including the key issues of the present research, i.e. the flavor structure of the sea-quark distribution in the nucleon. We hope that these characteristic predictions reported in the present paper will be tested through more elaborate analyses of the neutrino-induced DIS measurements, the semi-inclusive DIS measurements, the polarized Drell-Yan processes in  $pp$  or  $p\bar{p}$  collisions, etc., to be carried out in the near future.

## ACKNOWLEDGMENTS

The author would like to thank Y. Nakakoji for his helpful collaboration at the early stage on the investigation of the charge-symmetry-violating parton distributions. He also greatly acknowledges useful discussions with J.-C. Peng and K.-F. Liu at the workshop “Flavor Structure of the Nucleon Sea” held at ECT\* in July, 2013.

- 
- [1] T. Muta, *Foundations of Quantum Chromodynamics* (World Scientific, Singapore, 1998).
  - [2] J. Collins, *Foundations of Perturbative QCD* (Cambridge University Press, New York, 2011).
  - [3] M. Anselmino, A. Efremov, and E. Leader, *Phys. Rep.* **261**, 1 (1995).
  - [4] B. Lampe and E. Reya, *Phys. Rep.* **332**, 1 (2000).
  - [5] P. Jimenez-Delgado, W. Melnitchouk, and F. Owens, *J. Phys. G : Nucl. Part. Phys.* **40**, 093102 (2013).
  - [6] NMC Collaboration, P. Amaudruz et al., *Phys. Rev. Lett.* **66**, 2712 (1991).
  - [7] S. Kumano, *Phys. Rep.* **303**, 183 (1998).
  - [8] G.T. Garvey and J.-C. Peng, *Prog. Part. Nucl. Phys.* **47**, 204 (2001).
  - [9] J.-C. Peng and J.-W. Qiu, *Prog. Part. Nucl. Phys.* **76**, 43 (2014).
  - [10] J.D. Sullivan, *Phys. Rev. D* **5**, 1732 (1972).
  - [11] J.J. Aubert et al., *Phys. Lett. B* **123**, 275 (1983).
  - [12] S. Kumano, *Phys. Rev. D* **43**, 3067 (1991).
  - [13] S. Kumano and J.T. Londergan, *Phys. Rev. D* **44**, 717 (1991).
  - [14] M. Wakamatsu, *Phys. Rev. D* **44**, R2631 (1991).
  - [15] M. Wakamatsu, *Phys. Rev. D* **46**, 3762 (1992).
  - [16] W.-Y.P. Hwang, J. Speth, and G.E. Brown, *Z. Phys. A* **339**, 383 (1991).
  - [17] W. Koepf, L.L. Frankfurt, M. Strikman, *Phys. Rev. D* **53**, 2586 (1996).
  - [18] CCFR Collabotation, A. Bazarko et al, *Z. Phys. C* **65**, 189 (1995).
  - [19] CCFR/NuTeV Collaboration, Un-Ki Yang et al., *Phys. Rev. Lett.* **86**, 2742 (2001).
  - [20] V. Barone, C. Pascaud, and F. Zomer, *Eur. Phys. J. C* **12**, 243 (2000).
  - [21] NNPDF Collabotation, R.D. Ball et al., *Nucl. Phys. B* **823**, 195 (2009).
  - [22] A. Alekhin, S. Kulagin, and R. Petti, *Phys. Lett. B* **675**, 433 (2009).

- [23] I. Schienbein, J.Y. Yu, C. Keppel, J.G. Morfín, F.I. Olness, and J.F. Owens, Phys. Rev. D **77**, 054013 (2008).
- [24] I. Schienbein, J.Y. Yu, K. Kovařík, C. Keppel, J.G. Morfín, F.I. Olness, and J.F. Owens, Phys. Rev. D **80**, 094004 (2009).
- [25] HERMES Collaboration, A. Airapetian et al., Phys. Lett. B **666**, 446 (2008).
- [26] HERMES Collaboration, A. Airapetian et al., Phys. Rev. D **71**, 012003 (2005).
- [27] HERMES Collaboration, K. Ackerstaff et al., Phys. Lett. B **464**, 123 (1999).
- [28] COMPASS Collaboration, M. Alekseev et al., Phys. Lett. B **680**, 217 (2009).
- [29] COMPASS Collaboration, M. Alekseev et al., Phys. Lett. B **660**, 458 (2008).
- [30] D. de Florian, R. Sassot, M. Stratmann, Phys. Rev. D **75**, 114010 (2007).
- [31] D. de Florian, R. Sassot, M. Stratmann, Phys. Rev. D **76**, 074033 (2007).
- [32] S. Kretzer, Phys. Rev. D **62**, 054001 (2000).
- [33] M. Hirai, S. Kumano, T.-H. Nagai, and K. Sudoh, Phys. Rev. D **75**, 094009 (2007).
- [34] S. Albino, B.A. Kniehl, and G. Kramer, Nucl Phys. B **803**, 42 (2008).
- [35] Belle Collaboration, R. Seidl et al., Phys. Rev. D **78**, 032011 (2008).
- [36] D.I. Diakonov, V.Yu. Petrov, and P.V. Pobylitsa, Nucl. Phys. B **306**, 809 (1988).
- [37] M. Wakamatsu and H. Yoshiki, Nucl. Phys. A **524**, 561 (1991).
- [38] S. Kahana and G. Ripka, Nucl. Phys. A **429**, 462 (1984).
- [39] M. Wakamatsu, Prog. Theor. Phys. Suppl. **109**, 115 (1992).
- [40] Chr.V. Christov, A. Blotz, H.-C. Kim, P.V. Pobylitsa, T. Wakabe, Th. Meissner, E.Ruiz Arriola, and K. Goeke, Prog. Theor. Nucl. Part. Phys. **37**, 91 (1996).
- [41] R. Alkofer, H. Reinhardt, and H. Weigel, Phys. Rep. **265**, 139 (1996).
- [42] D.I. Diakonov and V.Yu. Petrov, *At the Frontier of Particle Physics* (World Scientific, Singapore, 2001), Vol.1.
- [43] D.I. Diakonov, V.Yu. Petrov, P.V. Pobylitsa, M.V. Polyakov, and C. Weiss, Nucl. Phys. B **480**, 341 (1996).
- [44] D.I. Diakonov, V.Yu. Petrov, P.V. Pobylitsa, M.V. Polyakov, and C. Weiss, Phys. Rev. D **56**, 4069 (1997).
- [45] P.V. Pobylitsa, M.V. Polyakov, K. Goeke, T. Watabe, and C. Weiss, Phys. Rev. D **59**, 034024 (1999).
- [46] H. Weigel, L. Gamberg, and H.Reinhardt, Mod. Phys. Lett. A **11**, 3021 (1996).

- [47] H. Weigel, L. Gamberg, and H.Reinhardt, Phys. Lett. B **399**, 286 (1997).
- [48] L. Gamberg, H. Reinhardt, and H. Weigel, Phys. Rev. D **58**, 054014 (1998).
- [49] M. Wakamatsu and T. Kubota, Phys. Rev. D **57**, 5755 (1998).
- [50] M. Wakamatsu and T. Kubota, Phys. Rev. D **60**, 034020 (1999).
- [51] M. Wakamatsu and T. Watabe, Phys. Rev. D **62**, 054009 (2000).
- [52] M. Wakamatsu, Phys. Rev. D **67**, 034005 (2003).
- [53] M. Wakamatsu, Phys. Rev. D **67**, 034006 (2003).
- [54] H. Chen, F.-G. Cao, and A.I. Signal, J. Phys. G : Nucl. Part. Phys. **37**, 105006 (2010).
- [55] F.-G. Cao and A.I. Signal, Phys. Lett. B **559**, 220 (2003).
- [56] NuTeV Collaboration, G.P. Zeller et al., Phys. Rev. Lett. **88**, 091802 (2002).
- [57] NuTeV Collaboration, G.P. Zeller et al., Phys. Rev. D **65**, 111103 (2002).
- [58] A.I. Signal and A.W. Thomas, Phys. Lett. B **191**, 205 (1987).
- [59] M. Burkardt and B.J. Warr, Phys. Rev D **45**, 958 (1992).
- [60] S.J. Brodsky and B.-Q. Ma, Phys. Lett. B **381**, 317 (1996).
- [61] Y. Ding and B.-Q. Ma, Phys. Lett. B **590**, 216 (2004).
- [62] J. Alwall and G. Ingelman, Phys. Rev. D **70**, 111505 (2004).
- [63] M. Wakamatsu. Phys. Rev. D **71**, 057504 (2005).
- [64] Y. Ding, R.-G. Xu, and B.-Q. Ma, Phys. Lett. B **607**, 101 (2005).
- [65] J.T. Londergan and A.W. Thomas, J. Phys. G : Nucl. Part. Phys. **31**, 1151 (2005).
- [66] J.T. Londergan, J.C. Peng, and A.W. Thomas, Rev. Mod. Phys. **82**, 2009 (2010).
- [67] Eric Sather, Phys. Lett. B **274**, 433 (1992).
- [68] E. Rodionov, A.W. Thomas, and J.T. Londergan, Mod. Phys. Lett. A **9**, 1799 (1994).
- [69] J.T. Londergan and A.W. Thomas, Phys. Lett. B **558**, 132 (2003).
- [70] M. Glúck, P. Jimenez-Delgado, and E. Reya, Phys. Rev. Lett. **95**, 022002 (2005).
- [71] A.D. Martin, R.G. Roberts, W.J. Stirling, and R.S. Thorne, Eur. Phys. J. C **39**, 155 (2005).
- [72] CSSM and QCDSF/UKQCD Collaborations, R. Horsley et al.,  
Phys. Rev. D **83**, 051501(R) (2011).
- [73] NNPDF Collaboration, R.D. Ball et al., Nucl. Phys. B **855**, 153 (2012).
- [74] NNPDF Collaboration, R.D. Ball et al, Nucl. Phys. B **855**, 153 (2012).
- [75] A. Blotz, D. Diakonov, K. Goeke, N.W. Park, V. Petrov, and P.V. Pobylitsa,  
Nucl. Phys. A **555**, 765 (1993).

- [76] E. Witten, Nucl. Phys. B **223**, 422, 433 (1983).
- [77] M.A. Nowak, P.O. Mazur, and M. Praszalowicz, Phys. Lett. B **147**, 137 (1984).
- [78] E. Guadagnini, Nucl. Phys. B **236**, 35 (1985).
- [79] D.I. Diakonov and V.Yu. Petrov, Nucl. Phys. B **272**, 457 (1986).
- [80] D.I. Diakonov, Prog. Part. Nucl. Phys. **51**, 173 (2003).
- [81] V.Yu. Petrov, P.V. Pobylitsa, M.V. Polyakov, I. Boring, K. Goeke, and C. Weiss, Phys. Rev. D **57**, 4325 (1998).
- [82] A.D. Martin, R.G. Roberts, W.J. Stirling, and R.S. Thorne, Eur. Phys. J. C **35**, 325 (2004).
- [83] A.D. Martin, W.J. Stirling, and R.S. Thorne, Phys. Lett. B **636**, 259, (2006).
- [84] P.J. Mulders and S.J. Pollock, Nucl. Phys. A **588**, 876 (1995).
- [85] E. Ruiz Arriola, Nucl. Phys. A **641**, 461 (1998).
- [86] H. Yabu and K. Ando, Nucl. Phys. B **301**, 601 (1988).
- [87] C.G. Callen, K. Hornbostel, and I. Klebanov, Phys. Lett. B **202**, 269 (1988).
- [88] J.P. Blaizot, M. Rho, and N.N. Scoccola, Phys. Lett. B **209**, 27 (1988).
- [89] W.-C. Chang and J.-C. Peng, Phys. Lett. B **666**, 446 (2011).
- [90] K.-F. Liu, W.-C. Chang, H.-Y. Cheng, and J.-C. Peng, Phys. Rev. Lett. **109**, 252002 (2012).
- [91] S.J. Brodsky, P. Hoyer, C. Peterson, and N. Sakai, Phys. Lett. B **93**, 451 (1980).
- [92] S.J. Brodsky, C. Peterson, and N. Sakai, Phys. Rev. D **23**, 2745 (1981).
- [93] CTEQ Collaboration, P.M. Nadolsky et al., Phys. Rev. D **78**, 013004 (2008).
- [94] H.L. Lai, M. Guzzi, J. Huston, Z. Li, P.M. Nadolsky, J. Pumplin, and C.P. Yuan, Phys. Rev. D **82**, 074024 (2010).
- [95] E. Leader, A.V. Sidorov, and D.B. Stamenov, arXiv : 1406.4678 [hep-ph] (2014).
- [96] HERMES Collaboration : A. Airapetian et al., Phys. Rev. D **89**, 097101 (2014).
- [97] M. Stolarski, arXiv : 1407.3721 [hep-ph] (2014).
- [98] W.-C. Chang and J.-C. Peng, Phys. Rev. Lett. **106**, 252002 (2011).
- [99] K.-F. Liu and S.J. Dong, Phys. Rev. Lett. **72**, 1790 (1994).
- [100] K.-F. Liu, Phys. Rev. D **62**, 074501 (2000).
- [101] A.V. Efremov, K. Goeke, and P.V. Pobylitsa, Phys. Lett. B **488**, 182 (2000).
- [102] D. de Florian, R. Sassot, M. Stratmann, and W. Vogelsang, arXiv:1404.4293 [hep-ph] (2014).
- [103] D. de Florian, R. Sassot, M. Stratmann, and W. Vogelsang, Phys. Rev. Lett. **101**, 072001 (2008).

- [104] D. de Florian, R. Sassot, M. Stratmann, and W. Vogelsang, *Phys. Rev. D* **80**, 034030 (2009).
- [105] B. Dressler, K. Goeke, M.V. Polyakov, and C. Weiss, *Eur. Phys. J. C* **14**, 147 (2000)
- [106] A. Blotz, M. Praszalowicz, and K. Goeke, *Phys. Rev. D* **53**, 485 (1996).
- [107] M. Wakamatsu and N. Kaya, *Prog. Theor. Phys.* **95**, 767 (1996).
- [108] F.-G. Cao and A.I. Signal, *Eur. Phys. J. C* **21**, 105 (2001).
- [109] C.J. Benesh and T. Goldman, *Phys. Rev. C* **55**, 441 (1997).